Power and Discrete Rate Adaptation in Wideband NOMA in Frequency-Selective Channels

S. Sruthy, *Student Member, IEEE* and Neelesh B. Mehta, *Fellow, IEEE*

Abstract

Power-domain non-orthogonal multiple access (NOMA) superimposes signals of multiple users and transmits them simultaneously. To be implemented in 5G and beyond orthogonal frequency division multiplexing systems, it must adhere to the constraint imposed by the standard that the same modulation and coding scheme (MCS) and power must be used across all physical resource blocks (PRBs) assigned to each user. However, the PRBs have different gains in wideband channels and the MCSs must belong to a discrete, pre-specified set. We propose a method that uses the exponential effective signal-to-noise ratio mapping (EESM) to systematically determine whether a feasible power allocation exists for a given choice of MCSs, and to find the MCSs that maximize the weighted sum rate for multiple user NOMA. We then propose a novel power-normalized EESM with backtracking (PB) method. It develops and exploits explicit analytical criteria to check for feasibility. We prove that it is a relaxation of the original problem under various conditions and is exact for narrowband channels. The average weighted sum rate of PB is indistinguishable from that of the EESM-used method despite its lower complexity. It is higher than that of wideband orthogonal multiple access, which is currently employed by 5G.

Index Terms

Non-orthogonal multiple access (NOMA), wideband, adaptive modulation and coding, power allocation, exponential effective signal-to-noise ratio mapping.

S. Sruthy and N. B. Mehta are with the Electrical Communication Engineering department, Indian Institute of Science, Bengaluru, India (Emails: sruthys@iisc.ac.in, nbmehta@iisc.ac.in).

A part of this paper has been accepted in the IEEE International Conference on Communications (ICC), May 2023 [1].

Power and Discrete Rate Adaptation in Wideband NOMA in Frequency-Selective Channels

I. Introduction

Several technologies such as full-duplex radio, sidelink communications, massive multi-antenna systems, network controlled relaying, and non-orthogonal multiple access (NOMA) are being pursued for 5G new radio (NR) and beyond wireless systems. NOMA enables a base station (BS) to serve multiple users simultaneously over the same time-frequency resources [2].

In downlink power-domain NOMA, the BS superimposes signals of two or more users with different transmit powers and transmits them simultaneously [3]. One or more of these users employ successive interference cancellation (SIC) in their receivers to retrieve their data in the presence of interference from the other users' signals. For example, in two-user NOMA that operates in the SIC-stable regime, the near user first decodes the far user's data, cancels it from its received signal, and decodes its own signal. On the other hand, the far user decodes its data by considering the near user's signal as interference. To facilitate this, the far user is allocated a higher transmit power than the near user. However, from an information-theoretic perspective, the constraint that the near user must be allocated a lower transmission power than the far user is not required [4, Ch. 6].

NOMA improves spectral efficiency and user fairness, lowers the transmission delay, and achieves a higher cell-edge throughput than orthogonal multiple access (OMA). To be implemented in 5G NR and beyond standards, NOMA must operate in combination with orthogonal frequency division multiplexing (OFDM), which is the physical radio access technology in these standards. In OFDM, the system bandwidth is divided into physical resource blocks (PRBs). Each PRB consists of 12 subcarriers and has a bandwidth of 180 to 2880 kHz depending on

the numerology. The scheduler at the BS can assign multiple contiguous PRBs to each user depending on the data payload.

Given the large bandwidths that span several MHz, these systems often operate over frequency-selective channels in which the channel gain varies from one PRB to another. However, the standard mandates that the same modulation and coding scheme (MCS) and power must be used on all the subcarriers assigned to a user [5, Sec. 5.2.5.1]. Furthermore, the set of MCSs is finite. For example, 5G NR uses QPSK, 16-QAM, 64-QAM, and 256-QAM constellations with coding rates between $78/1024$ and $948/1024$ [6, Table 5.2.2.1-3]. This is done to limit uplink feedback and downlink control signaling overhead, which would otherwise increase with the system bandwidth. Therefore, the BS scheduler needs to determine which users to pair, which PRBs to assign to them, and which single MCS and power to assign to each user. We shall refer to NOMA in which transmissions span multiple PRBs and are subject to the above common MCS and power constraint as *wideband NOMA*.

A. Literature on NOMA in Multi-carrier Systems

A wealth of literature on NOMA has focused on frequency-flat channels (see [2], [7]–[11] and the references therein), in which the channel gains of all subcarriers are the same. We focus our discussion below on NOMA in multi-carrier systems.

Power allocation and continuous rate adaptation are done on a per-subcarrier basis in [12]–[15] and the references therein. Bit loading with variable number of bits per subcarrier is studied in [16] and [17] for fixed and continuous power allocation, respectively. User pairing and subcarrier allocation are also done in [17]. Joint power and subcarrier allocation to maximize the weighted sum rate of multi-carrier NOMA is considered in [18]–[20]. However, the rate and power are adapted on a per-subcarrier basis. A user pairing scheme for an OFDM-based cooperative NOMA is proposed in [21] assuming continuous rate adaptation per subcarrier and fixed power allocation. NOMA for OFDM-based visible light communication (VLC) systems is studied in [22]–[24]. However, continuous rate adaptation per subcarrier or subband is assumed.[1]

[1]A subband is a set of contiguous PRBs.

System-level simulation results that compare NOMA and OMA with discrete rate adaptation are presented in [25]. However, open-loop fractional transmit power control (FTPC) is employed. System-level simulations of average and cell-edge user throughput of a wideband NOMA scheduler, which jointly does user pairing, power allocation, and MCS selection, are presented in [26]. Mutual information effective signal-to-interference-noise ratio (SINR) mapping (MIESM) is used to determine the MCS and power allocation. A dynamic power allocation method is proposed in [27] for continuous rate adaptation.

B. Contributions

We develop the theory for power and discrete rate adaptation for downlink wideband NOMA for the SIC-stable and information-theoretic regimes. The transmission to each user is subject to a block error rate (BLER) constraint, since a coded block of data is sent. A key difference compared to the literature is that the MCS selection and the power allocation are the same for all the PRBs allocated to each user, as mandated by the 5G NR standard. We make the following contributions.

- We present an effective SINR-based approach to determine the optimal MCSs and powers of the superimposed users to maximize the weighted sum rate. It uses the exponential effective SINR mapping (EESM) link quality metric to systematically map the vector of SINRs of each user to a single equivalent flat-fading SINR. EESM leads to MCS-specific decoding constraints that are non-linear functions of the powers of the users. We propose a gradient-descent algorithm based on a barrier function to numerically find a feasible power allocation for a given choice of MCSs. Among the MCSs for which a feasible power allocation exists, the one with the largest weighted sum rate is the optimal one.
- We then present a novel lower-complexity method called power-normalized EESM (PNEESM) in which the decoding constraints become linear inequalities in the users' powers. This leads to closed-form criteria that explicitly identify whether a feasible solution exists and eliminate numerical searches altogether. We show that the PNEESM method is a relaxation of the original optimization problem under various conditions. Furthermore, this relaxation is tight in the sense that it is exact for narrowband channels.

- Since a relaxation may result to a solution that is infeasible for the original optimization problem, we propose a PNEESM with backtracking (PB) algorithm, which arrives at a feasible solution from an infeasible one. PB entails far fewer numerical searches than the brute-force approach to find the optimal MCSs of the users. This low complexity is beneficial for the scheduler that also needs to do user pairing and PRB allocation.
- We present an analysis of the average weighted sum rate of the PNEESM method using recent results on the statistics of EESM [28].
- Our numerical results that show that the average weighted sum rate of PB is indistinguishable from that of the more involved effective SINR-based approach. We find that wideband NOMA achieves a higher average weighted sum rate than wideband OMA, which is the analogue of OMA in wideband channels and is currently employed by 5G NR. We find that the per-PRB and continuous rate adaptation models overestimate the performance of NOMA.

C. Comparison with Literature

Our work differs from the literature in many respects. First, [2], [7]–[10] assume a flat-fading channel. While [12]–[27] consider multi-carrier NOMA over a frequency-selective channel, they adapt the MCS and the power on a per-subcarrier or per-subband basis. On the other hand, we assume a frequency-selective channel and assign the same MCS and power for all the PRBs allocated to each user, as mandated by the standard. Second, [7], [8], [10], [12]–[15], [18]–[24], [29] assume continuous rate adaptation based on the Shannon capacity formula. This is an idealization because the standard permits the BS to choose only from a pre-specified finite set of MCSs. Third, [8], [10], [13], [16], [21], [25], [29] use fixed transmit power allocation or FTPC, which is not a function of the channel realizations and the MCSs of the users. While [25] considers wideband channels, it takes the arithmetic average of the subband SINRs to be the effective SINR. This is known to underestimate the BLER [30]. In [26], the focus is on simulations and the power adaptation requires an involved numerical search. Table I summarizes how the literature differs from our work.

TABLE I

COMPARISON OF LITERATURE ON POWER ALLOCATION AND RATE ADAPTATION IN MULTI-CARRIER NOMA

Reference	*Rate adaptation*	*Frequency resolution*	*Transmit power allocation*
Yuan et al. [12], Li et al. [14] Ou et al. [15]	Continuous	Per subcarrier	Dynamic
Mcwade et al. [13], Cheng et al. [21]	Continuous	Per subcarrier	Fixed
Assaf et al. [16]	Discrete	Per subcarrier	Fixed
Tseng et al. [17]	Discrete	Per subcarrier	Dynamic
Lei et al. [18], Salaun et al. [19] Fu et al. [20], Liu et al. [27]	Continuous	Per subcarrier	Dynamic
Wang et al. [22], Fu et al. [23] (VLC)	Continuous	Per subcarrier	Dynamic
Feng et al. [24] (VLC)	Continuous	Per subband	Dynamic
Saito et al. [25]	Discrete	Per subband	FTPC
Thieu et al. [26]	Discrete	Wideband	Dynamic (numerical search)
This manuscript	Discrete	Wideband	Dynamic

D. Outline and Notations

Section II describes the system model for downlink wideband NOMA. Section III presents the approach for power allocation and MCS selection for two users, and analyzes the average weighted sum rate of the PNEESM method. Section IV extends the approach to three and more users. Numerical results are presented in Section V, and our conclusions follow in Section VI.

Notations: We show scalar variables in normal font and vector variables in bold font. $\Pr(A)$ denotes the probability of an event A, and $\mathbb{E}[.]$ denotes the expectation. A^C represents the complement of the event A. The cumulative distribution function (CDF) and probability density function (PDF) of a random variable (RV) X are denoted by $F_X(.)$ and $f_X(.)$, respectively.

II. SYSTEM MODEL AND PROBLEM STATEMENT

We consider a set of N PRBs over which the BS simultaneously serves K users using NOMA. We first focus on the $K = 2$ case. The case with $K = 3$ and more users is discussed in Section IV. Our approach applies to any allocation of the users to the PRBs by the scheduler at the BS. We note that OMA, which is used in today's systems, allocates only one user to the set of PRBs. The system model is illustrated in Figure 1.

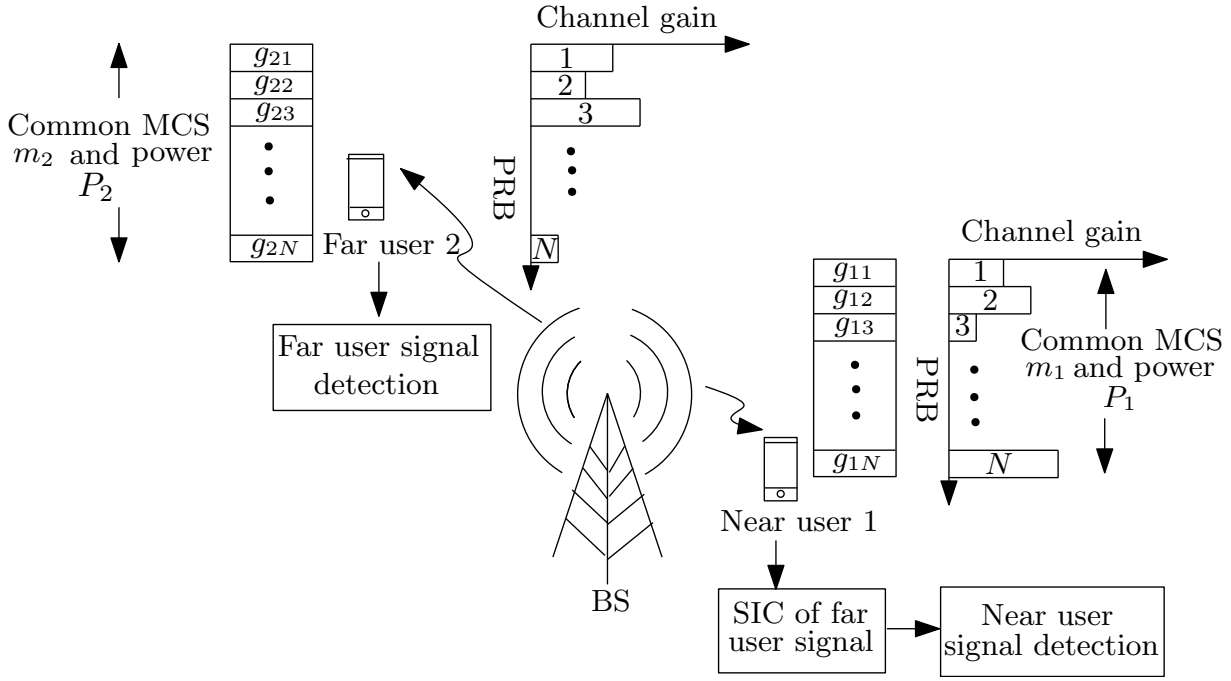

Fig. 1. System model for wideband NOMA with near and far users in the SIC-stable regime. Shown for each user are its PRB gains, common MCS, and common power.

The BS transmits with a power P per subcarrier. It transmits the superimposed signal of the two users across these N PRBs. The transmit powers of users 1 and 2 are P_1 and P_2, respectively. In the SIC-stable regime, $P_1 < P_2$. This ensures that error propagation does not happen during SIC [29]. In the information-theoretic regime, no such ordering constraint is imposed on P_1 and P_2.

Let g_{kn} denote baseband channel power gain (with unit mean) between the k^{th} user and the BS on the n^{th} PRB, for $1 \leq k \leq K$ and $1 \leq n \leq N$, and $\mathbf{g}_k = [g_{k1}, g_{k2}, \ldots, g_{kN}]$. The channel is flat over a PRB. This is reasonable when the PRB bandwidth is less than the coherence bandwidth of the channel. Let N_0 denote the noise power spectral density, B be the subcarrier bandwidth, and ℓ_k be the pathloss for the k^{th} user.

The SINR of all subcarriers in PRB n is $\gamma_{12}^{(n)}$ of user 1 when it decodes user 2's data is given by $\gamma_{12}^{(n)} = \frac{P_2 \ell_1 g_{1n}}{P_1 \ell_1 g_{1n} + N_0 B}$. The SINR $\gamma_{11}^{(n)}$ of PRB n of user 1 after canceling user 2's interference for decoding its own data is $\gamma_{11}^{(n)} = \frac{P_1 \ell_1 g_{1n}}{N_0 B}$. And, the SINR $\gamma_{22}^{(n)}$ of user 2 of PRB n when it decodes its own data is $\gamma_{22}^{(n)} = \frac{P_2 \ell_2 g_{2n}}{P_1 \ell_2 g_{2n} + N_0 B}$. Let $\mathbf{\Gamma}_{kj} = [\gamma_{kj}^{(1)}, \gamma_{kj}^{(2)}, \ldots, \gamma_{kj}^{(N)}]$ denote the vector of

SINRs of the k^{th} user when it decodes the j^{th} user's data, for $(k,j) \in \{(1,1),(1,2),(2,2)\}$.

Let $\Omega = \{0,1,2,\ldots,L\}$ denote the discrete set of MCSs that can be used for transmission. The information rate of MCS $m \in \Omega$ is r_m. The MCSs are arranged in the increasing order of their rates: $0 = r_0 < r_1 < r_2 < \cdots < r_L$. Here, MCS 0, which has a rate $r_0 = 0$, means that no transmission occurs. We focus on a single-input-single-output system, given that wideband NOMA has not been fully investigated in the literature even for it.

A. Problem Statement

Our goal is to maximize the weighted sum rate by choosing the MCS $m_1 \in \Omega$ of user 1 and the MCS m_2 of user 2 and their powers. Let $\mathsf{BLER}_m\left(\mathbf{\Gamma}_{kj}\right)$ denote the BLER of MCS m when it is transmitted over N PRBs whose vector of SINRs is $\mathbf{\Gamma}_{kj}$. The optimum MCSs and powers are the solution to the following constrained optimization problem:

$$\mathcal{S}_0 : \max_{\substack{m_1\in\Omega, m_2\in\Omega,\\ P_1\geq 0, P_2\geq 0}} \quad \{r_{m_1} + w_2 r_{m_2}\}, \tag{1}$$

$$\text{s.t.} \quad \mathsf{BLER}_{m_1}(\mathbf{\Gamma}_{11}) \leq \epsilon, \tag{2}$$

$$\max\{\mathsf{BLER}_{m_2}(\mathbf{\Gamma}_{12}), \mathsf{BLER}_{m_2}(\mathbf{\Gamma}_{22})\} \leq \epsilon, \tag{3}$$

$$P_1 + P_2 = P, \tag{4}$$

$$P_1 < P_2, \text{ if } m_2 > 0, \tag{5}$$

where $w_2 \geq 1$ is the weight for user 2. When $w_2 = 1$, the objective function reduces to $r_{m_1} + r_{m_2}$, which is the sum rate. Making $w_2 > 1$ incentivizes the resource allocation algorithm to increase r_{m_2} because any change in it is amplified by w_2. This leads to higher rates being assigned to the far user, which improves fairness. This approach can be generalized to incorporate other utility functions such as the α-fair utility function, which has proportional fairness and max-min fairness as its special cases.

The constraint in (2) requires that the BLER of user 1 when it decodes its block of data should be less than or equal to the target value ϵ. The constraint in (3) requires that the BLERs of users 1 and 2 when they decode user 2's block of data should be less than or equal to ϵ. For example, cellular systems operate at an error target of 0.1 [6]. The total power constraint

and the SIC-stable regime's constraint are captured in (4) and (5), respectively. Given (4), the constraint in (5) is equivalent to $P_1 < \frac{P}{2}$. However, when the BS does not transmit to user 2, no such constraint is required.

For a given MCS pair (m_1, m_2), we say that a feasible power pair exists if it satisfies the above constraints. If such a feasible power pair exists, then we say that the MCS pair (m_1, m_2) is feasible. The problem formulation is the same for the information-theoretic regime, except that the constraint in (5) is removed.

III. Systematic Approach for Joint Power and Rate Adaptation

$\mathcal{S}_0$ is intractable because the BLER of an MCS when it is transmitted over N PRBs with different SINRs is not available in closed-form. We address this by using EESM, which maps a vector of SINRs into an equivalent effective SINR with the same BLER over an additive white Gaussian noise (AWGN) channel. EESM has been extensively used in 3GPP system simulations and for generating channel quality feedback due to its accuracy [31]. For a vector of SINRs $\mathbf{x} = [x_1, x_2, \ldots, x_N]$, the effective SINR of MCS m, which we denote by $\mathsf{EESM}(\mathbf{x}, \beta_m)$, is defined as

$$\mathsf{EESM}(\mathbf{x}, \beta_m) = -\beta_m \ln\left(\frac{1}{N}\sum_{n=1}^{N} \exp\left(-\frac{x_n}{\beta_m}\right)\right), \tag{6}$$

where β_m is an MCS-dependent scaling constant that is available in the literature [32, Table 1]. β_m increases as the MCS rate r_m, or equivalently the index m, increases.

Comment: MIESM has also been used as a link quality metric in 3GPP system simulations. However, its involved form, which involves a single integral, makes it intractable. EESM and MIESM avoid the pitfalls of simpler alternate approaches that take the minimum SINR or arithmetic mean or geometric mean of the PRB SINRs as the effective SINR. The minimum SINR approach is too conservative, while the arithmetic and geometric means are known to overestimate the effective SINR and underestimate the BLER [28], [30].

Let $\tilde{\Gamma}_{kj}(m)$ be the effective SINR of the k^{th} user when it decodes the j^{th} user's data that uses MCS m. From (6), we get

$$\tilde{\Gamma}_{kj}(m) = -\beta_m \ln\left(\frac{1}{N}\sum_{n=1}^{N} \exp\left[-\frac{\gamma_{kj}^{(n)}}{\beta_m}\right]\right). \tag{7}$$

Let T_m be the smallest SINR at which the BLER of MCS m in an additive white Gaussian noise channel is equal to ϵ. Then, (2) is equivalent to $\tilde{\Gamma}_{11}(m_1) \geq T_{m_1}$. And, (3) is equivalent to $\min\{\tilde{\Gamma}_{12}(m_2), \tilde{\Gamma}_{22}(m_2)\} \geq T_{m_2}$. Hence, $\mathcal{S}_0$ is equivalent to the following problem $\mathcal{S}_1$:

$$\mathcal{S}_1 : \max_{\substack{m_1\in\Omega, m_2\in\Omega,\\ P_1\geq 0, P_2\geq 0}} \quad \{r_{m_1} + w_2 r_{m_2}\}, \tag{8}$$

$$\text{s.t.} \quad \tilde{\Gamma}_{11}(m_1) \geq T_{m_1}, \tag{9}$$

$$\min\{\tilde{\Gamma}_{12}(m_2), \tilde{\Gamma}_{22}(m_2)\} \geq T_{m_2}, \tag{10}$$

$$P_1 + P_2 = P, \tag{11}$$

$$P_1 < \frac{P}{2}, \text{ if } m_2 > 0. \tag{12}$$

In (10), the effective SINR $\tilde{\Gamma}_{12}(m_2)$ of the near user 1 is greater than that of the far user 2, $\tilde{\Gamma}_{22}(m_2)$, with a high probability since the near user is closer to the BS. Hence, (10) simplifies to $\tilde{\Gamma}_{22}(m_2) \geq T_{m_2}$. To solve $\mathcal{S}_1$, for every MCS pair, we determine if a feasible power pair exists. Then, among the feasible MCS pairs, the one with the largest weighted sum rate is the optimal one.

A. Existence of a Feasible Power Allocation Given an MCS Choice

We present a barrier function based approach below to numerically assess if a feasible (P_1, P_2) exists [33, Ch. 11]. The barrier function F consists of three exponential terms that are based on the constraints in (9), (10), and (12):

$$F(P_1) = \exp\left(-\left[\tilde{\Gamma}_{11}(m_1) - T_{m_1}\right]\right) + \exp\left(-\left[\tilde{\Gamma}_{22}(m_2) - T_{m_2}\right]\right) + \exp\left(-\left[\frac{P}{2} - P_1\right]\right). \tag{13}$$

Here, $\exp(-x)$ is an approximation to the indicator function [33]. It is non-negative and increases rapidly if the inequality is not satisfied, i.e., when $x < 0$. For a feasible solution, F is small. We find the P_1 and $P_2 = P - P_1$ that minimize F using gradient descent and check if they satisfy the constraints of $\mathcal{S}_1$. For $m_2 = 0$, the third term in (13) is absent.

The update equation in gradient descent at the $(k+1)^{\text{th}}$ iteration can be written as $P_1^{(k+1)} = P_1^{(k)} - \eta \frac{\partial F}{\partial P_1^{(k)}}$, where η is the learning rate and $P_1^{(k)}$ is the power at the k^{th} step. Gradient descent terminates when the difference in the values of F at two consecutive iterations is less than a

predetermined threshold or $P_1^{(k)}$ satisfies all the constraints of $\mathcal{S}_1$. We can prove that F is a L-Lipschitz function. We skip the proof to conserve space. Hence, gradient descent is guaranteed to converge to a stationary point so long as $\eta < \frac{2}{L}$ [34, Ch. 1].[2] For the information-theoretic regime, the approach is similar except that F consists of only the first two terms in (13).

B. Analytical Method that Avoids Numerical Search

The above numerical search for a feasible (P_1, P_2) needs to be done for every realization of the vector of channel power gains of users 1 and 2 and for every MCS pair (m_1, m_2). In order to avoid this, we propose an alternate and novel approach based on PNEESM. The PNEESM $\tilde{G}_k(m)$ of the k^{th} user when it uses MCS m is defined as

$$\tilde{G}_k(m) = -\beta_m \ln\left(\frac{1}{N}\sum_{n=1}^{N}\exp\left(-\frac{\alpha \ell_k g_{kn}}{N_0 B \beta_m}\right)\right), \text{ for } k \in \{1,2\}, \tag{14}$$

where α is a pre-specified positive constant. $\tilde{G}_k(m)$ has the same form as EESM except that the power term is replaced with the constant α. We first state the following property of PNEESM.

Lemma *1:* The PNEESM $\tilde{G}_k(m)$ increases as the MCS index m increases.

Proof: The proof is given in Appendix A. ■

The following two lemmas use Lemma 1 and connect the effective SINR $\tilde{\Gamma}_{kj}(m)$ and the PNEESM $\tilde{G}_k(m)$. Let $\overline{\mathsf{SNR}}_k = \frac{P_k \ell_2}{N_0 B N}\sum_{n=1}^{N} g_{2n}$ be the subcarrier-averaged signal-to-noise ratio (SNR) of the k^{th} user.

Lemma *2:* When β_{m_2} and $\overline{\mathsf{SNR}}_1$ are large, $\tilde{\Gamma}_{22}(m_2)$ is upper bounded by

$$\tilde{\Gamma}_{22}(m_2) \leq \frac{\frac{P_2}{\alpha}\tilde{G}_2(m_2)}{\frac{P_1}{\alpha}\tilde{G}_2(m_2)+1} + \frac{P_2}{P_1}\mathcal{O}\left(\frac{1}{\overline{\mathsf{SNR}}_1}\right). \tag{15}$$

When $\overline{\mathsf{SNR}}_1$ is small and $\frac{P_2}{\alpha} \geq 1$, $\tilde{\Gamma}_{22}(m_2)$ is upper bounded by

$$\tilde{\Gamma}_{22}(m_2) \leq \frac{\frac{P_2}{\alpha}\tilde{G}_2(m_2)}{\frac{P_1}{\alpha}\tilde{G}_2(m_2)+1}. \tag{16}$$

Proof: The proof is given in Appendix B. ■

[2]We note that F is not a convex function of P_1. The algorithm can terminate prematurely at a stationary point that is not a minima. However, this scenario did not occur in the simulations.

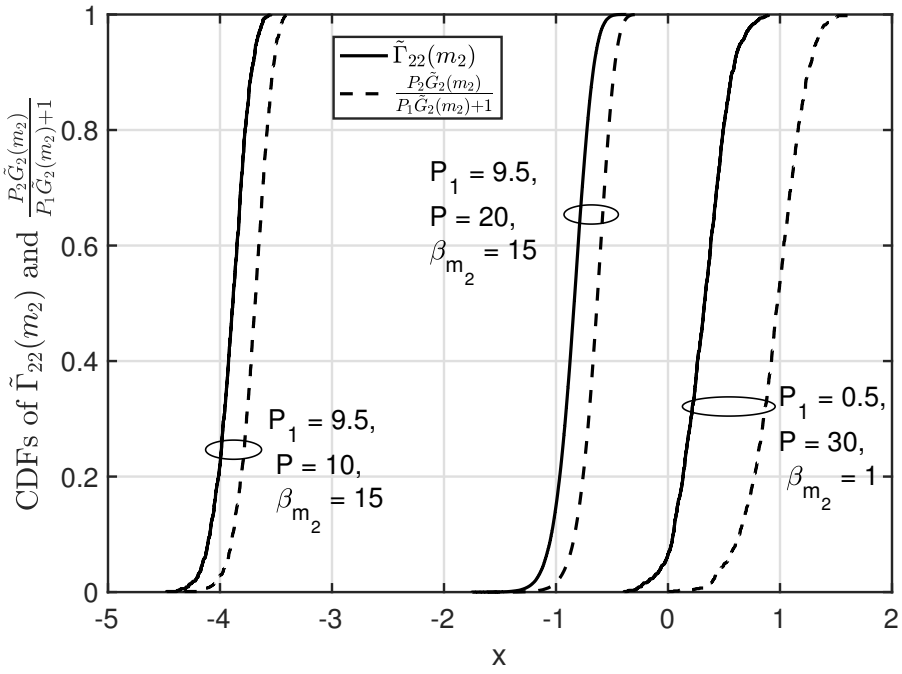

Fig. 2. CDFs of $\tilde{\Gamma}_{22}(m_2)$ and $\frac{P_2\tilde{G}_2(m_2)}{P_1\tilde{G}_2(m_2)+1}$ for small β_{m_2} and low $\overline{\mathsf{SNR}}_1$, large β_{m_2} and high $\overline{\mathsf{SNR}}_1$, and high $\overline{\mathsf{SNR}}_1$ and $P_2 < 1$ (α is normalized to 1).

Lemma *3:* The effective SINR $\tilde{\Gamma}_{11}(m_1)$ is upper bounded by

$$\tilde{\Gamma}_{11}(m_1) \leq \frac{P_1}{\alpha}\tilde{G}_1(m_1), \text{ for } \frac{P_1}{\alpha} \geq 1. \tag{17}$$

Proof: The proof is given in Appendix C. ■

We shall refer to $\frac{P_k}{\alpha}\tilde{G}_k(m)$ as the scaled PNEESM of the k^{th} user for MCS m. Here, α acts as a normalizing constant. Its value is inversely proportional to the ratio of the pathloss and the noise power. For $N = 1$, which is equivalent to the narrowband channel, we see that $\tilde{\Gamma}_{22}(m_2) = \frac{\frac{P_2}{\alpha}\tilde{G}_2(m_2)}{\frac{P_1}{\alpha}\tilde{G}_2(m_2)+1}$ and $\tilde{\Gamma}_{11}(m_1) = \frac{P_1}{\alpha}\tilde{G}_1(m_1)$, for all $\alpha > 0$. Thus, the inequalities become equalities, i.e., they are exact.

To verify Lemma 2 and also understand how often it applies even when the conditions specified in it do not hold, Figure 2 plots the empirical CDFs of $\tilde{\Gamma}_{22}(m_2)$ (in dB) and $\frac{P_2\tilde{G}_2(m_2)}{P_1\tilde{G}_2(m_2)+1}$ (in dB) for different values of β_{m_2} and powers. These CDFs are generated using 1000 realizations of the vectors of the channel gains of users 1 and 2. We see that the CDF of $\tilde{\Gamma}_{22}(m_2)$ is to the left of the CDF of $\frac{P_2\tilde{G}_2(m_2)}{P_1\tilde{G}_2(m_2)+1}$ not just for small β_{m_2} and low $\overline{\mathsf{SNR}}_1$ but also for high $\overline{\mathsf{SNR}}_1$ and

$P_2 < 1$. Therefore, the upper bound holds with high probability for all values of interest of β_m.[3]

When Lemma 2 holds, the constraint in (10) implies $\frac{P_2}{\alpha}\tilde{G}_2(m_2) \geq T_{m_2}\left(\frac{P_1}{\alpha}\tilde{G}_2(m_2)+1\right)$. Similarly, when Lemma 3 holds, the constraint in (9) implies $\frac{P_1}{\alpha}\tilde{G}_1(m_1) \geq T_{m_1}$. This leads to the following relaxation of $\mathcal{S}_1$, in which the constraints in (9) and (10) are replaced with new constraints that are *linear functions* of P_1 and P_2:

$$\mathcal{S}_2 : \max_{\substack{m_1\in\Omega, m_2\in\Omega,\\ P_1\geq 0, P_2\geq 0}} \quad \{r_{m_1} + w_2 r_{m_2}\}, \tag{18}$$

$$\text{s.t.} \quad \frac{P_1}{\alpha}\tilde{G}_1(m_1) \geq T_{m_1}, \tag{19}$$

$$\frac{P_2}{\alpha}\tilde{G}_2(m_2) \geq T_{m_2}\left(\frac{P_1}{\alpha}\tilde{G}_2(m_2)+1\right), \tag{20}$$

$$P_1 + P_2 = P, \tag{21}$$

$$P_1 < \frac{P}{2}, \text{ if } m_2 > 0. \tag{22}$$

The following result explicitly specifies when a feasible (P_1, P_2) exists for $\mathcal{S}_2$ for a given MCS pair (m_1, m_2). Thus, determining whether a feasible power allocation exists no longer requires a numerical search.

Result *1:* For an MCS pair (m_1, m_2), a feasible power allocation for the PNEESM method exists if and only if

$$\tilde{G}_1(m_1) > \max\left\{\frac{\alpha T_{m_1}\tilde{G}_2(m_2)(T_{m_2}+1)}{\tilde{G}_2(m_2)P - \alpha T_{m_2}}, \frac{2\alpha T_{m_1}}{P}\right\} \text{ and} \tag{23}$$

$$\tilde{G}_2(m_2) \geq \frac{\alpha T_{m_2}}{P}. \tag{24}$$

Proof: The proof is given in Appendix D. ■

For the information-theoretic regime, the corresponding result can be shown to be

$$\tilde{G}_1(m_1) > \frac{\alpha T_{m_1}\tilde{G}_2(m_2)(T_{m_2}+1)}{\tilde{G}_2(m_2)P - \alpha T_{m_2}} \text{ and } \tilde{G}_2(m_2) \geq \frac{\alpha T_{m_2}}{P}. \tag{25}$$

The solution obtained for $\mathcal{S}_2$ might be infeasible for $\mathcal{S}_1$, since it is a relaxation when both lemmas hold. Specifically, $\tilde{\Gamma}_{11}(m_1) \geq T_{m_1}$ implies that $\frac{P_1}{\alpha}\tilde{G}_1(m_1) \geq T_{m_1}$. However, the reverse need not be true since $\frac{P_1}{\alpha}\tilde{G}_1(m_1)$ upper bounds $\tilde{\Gamma}_{11}(m_1)$. Similarly, $\tilde{\Gamma}_{22}(m_2) \geq T_{m_2}$ implies

[3]We have observed that the upper bound is violated in only 5 out of 10^5 channel realizations.

Algorithm 1: Joint power and rate adaptation using PB

Input: $g_1\ell_1, g_2\ell_2, P, \alpha, \Omega$

Initialize: Set $\mathcal{Q} = \emptyset, \mathbf{m}_{\text{opt}} = (0, 0)$

for $(m_1, m_2) \in \Omega$ **do**

Determine $\tilde{G}_1(m_1)$ and $\tilde{G}_2(m_2)$;

if $\tilde{G}_1(m_1) > \max\left\{\frac{\alpha T_{m_1}\tilde{G}_2(m_2)(T_{m_2}+1)}{\tilde{G}_2(m_2)P-\alpha T_{m_2}}, \frac{2\alpha T_{m_1}}{P}\right\}$ & $\tilde{G}_2(m_2) \geq \frac{\alpha T_{m_2}}{P}$ **then**

$\mathcal{Q} = \mathcal{Q} \cup \{(m_1, m_2)\}$;

end

end

Repeat:

- Determine $\mathbf{m}_{\text{opt}}$ from $\mathcal{Q}$;
- Check feasibility of $\mathbf{m}_{\text{opt}}$ using barrier function method;

if $\mathbf{m}_{opt}$ *is feasible* **then**

Stop

else

$\mathcal{Q} \triangleq \mathcal{Q} \setminus \{\mathbf{m}_{\text{opt}}\}$;

end

Until: $\mathcal{Q} = \emptyset$**;**

that $\frac{P_2}{\alpha}\tilde{G}_2(m_2) \geq T_{m_2}\left(\frac{P_1}{\alpha}\tilde{G}_2(m_2) + 1\right)$, but the reverse may not hold. We present below an approach called PB to find a feasible solution from the infeasible solution so obtained.

Let $\mathcal{Q} = \{(m_1, m_2) \in \Omega \times \Omega : (m_1, m_2)$ is feasible$\}$ be the set of all MCS pairs that are feasible solutions of $\mathcal{S}_2$ for a given vector of channel realizations. $\mathcal{Q}$ can be easily determined by applying Result 1 to each MCS pair. Let $\mathbf{m}_{\text{opt}} = (m_1^*, m_2^*) \in \mathcal{Q}$ be the MCS pair with the largest weighted sum rate. Its feasibility is checked by applying the barrier function method of Section III-A. If it is feasible, then we are done. Else, we remove $\mathbf{m}_{\text{opt}}$ from $\mathcal{Q}$ and select the MCS pair with the largest weighted sum rate from $\mathcal{Q} \setminus \{\mathbf{m}_{\text{opt}}\}$. We then check its feasibility, and so on. The algorithm terminates when a feasible $\mathbf{m}_{\text{opt}}$ is found. Since $\mathcal{Q}$ is finite, the algorithm is guaranteed to terminate. The pseudo-code for the method is given in Algorithm 1.

Complexity Comparison: In the barrier function method, ascertaining the feasibility of an

MCS pair requires running a numerical routine for L^2 MCS pairs. On the other hand, in PB, the feasibility check needs to be done for only a handful of MCS pairs.

C. Analysis: Average Weighted Sum Rate of PNEESM Method

We now analyze the average weighted sum rate of the PNEESM method. The analysis enables an independent verification of the simulations and brings out the role of the system parameters. Let $R_{m_1,m_2} = r_{m_1} + w_2 r_{m_2}$. The average weighted sum rate $\bar{R}$ is given by

$$\bar{R} = \sum_{m_1=0}^{L} \sum_{m_2=0}^{L} R_{m_1,m_2} \text{Pr}\left(\mathbf{m}_{\text{opt}} = (m_1, m_2)\right). \tag{26}$$

Let $\mathcal{S}_{m_1,m_2}$ be the set of all MCS pairs whose weighted sum rate exceeds R_{m_1,m_2}. For (m_1, m_2) to be optimum, it must be feasible and every MCS pair in $\mathcal{S}_{m_1,m_2}$ must be infeasible. Thus,

$$\text{Pr}\left(\mathbf{m}_{\text{opt}} = (m_1, m_2)\right) = \text{Pr}((m_1, m_2) \text{ is feasible, MCS pairs in } \mathcal{S}_{m_1,m_2} \text{ are infeasible}). \tag{27}$$

The key challenge in evaluating the above probability is that the same vectors of SINRs decide whether an MCS pair in $\mathcal{S}_{m_1,m_2}$ is infeasible and whether $\mathbf{m}_{\text{opt}}$ is feasible. Hence, the above events are correlated. We address this below by considering a carefully chosen subset of $\mathcal{S}_{m_1,m_2}$.

Let $u \geq 0$ be the largest integer such that $R_{m_1-u,m_2+1} > R_{m_1,m_2}$, where $(m_1 - u, m_2 + 1) \in \mathcal{S}_{m_1,m_2}$. Similarly, let $v > 0$ be the smallest integer such that $R_{m_1+v,m_2-1} > R_{m_1,m_2}$, where $(m_1 + v, m_2 - 1) \in \mathcal{S}_{m_1,m_2}$. For ease of exposition, we deal with the boundary cases where no such u or v exists after we present Result 2. Then,

$$\text{Pr}\left(\mathbf{m}_{\text{opt}} = (m_1, m_2)\right) \leq \text{Pr}\left(E_1 \cap E_2^C \cap E_3^C \cap E_4^C\right), \tag{28}$$

where E_1, E_2, E_3, and E_4 denote the events that the MCS pairs (m_1, m_2), $(m_1 + 1, m_2)$, $(m_1 - u, m_2 + 1)$, and $(m_1 + v, m_2 - 1)$ are feasible, respectively. Using De Morgan's laws, we get

$$\begin{aligned}\text{Pr}\left(E_1 \cap E_2^C \cap E_3^C \cap E_4^C\right) &= \text{Pr}\left(E_1\right) - \text{Pr}\left(E_1 \cap E_2\right) - \text{Pr}\left(E_1 \cap E_3\right) - \text{Pr}\left(E_1 \cap E_4\right) \\ &+ \text{Pr}\left(E_1 \cap E_2 \cap E_3\right) + \text{Pr}\left(E_1 \cap E_2 \cap E_4\right) + \text{Pr}\left(E_1 \cap E_3 \cap E_4\right) - \text{Pr}\left(E_1 \cap E_2 \cap E_3 \cap E_4\right).\end{aligned} \tag{29}$$

In order to evaluate (29), we first present the following lemma about the statistics of $\tilde{G}_k(m)$.

Lemma *4:* The CDF $F_{\tilde{G}_k(m)}(x)$ and the PDF $f_{\tilde{G}_k(m)}(x)$ of $\tilde{G}_k(m)$ are given by

$$F_{\tilde{G}_k(m)}(x) = 1 - B_i\left(\exp\left(-\frac{x}{\beta_m}\right), a_m, b_m\right), \text{ for } x \geq 0, \tag{30}$$

$$f_{\tilde{G}_k(m)}(x) = \frac{\exp\left(-\frac{x}{\beta_m}\right)^{a_m}\left(1-\exp\left(-\frac{x}{\beta_m}\right)\right)^{(b_m-1)}}{\beta_m B(a_m, b_m)}, \text{ for } x \geq 0, \tag{31}$$

where B and B_i are the beta function and regularized incomplete beta function, respectively [35, Chs. 8.38, 8.39]. The beta parameters a_m and b_m are given by $a_m = \frac{\mathbb{E}[Y_{km}]\left(\mathbb{E}[Y_{km}]-\mathbb{E}\left[Y_{km}^2\right]\right)}{\mathbb{E}\left[Y_{km}^2\right]-(\mathbb{E}[Y_{km}])^2}$ and $b_m = \frac{(1-\mathbb{E}[Y_{km}])\left(\mathbb{E}[Y_{km}]-\mathbb{E}\left[Y_{km}^2\right]\right)}{\mathbb{E}\left[Y_{km}^2\right]-(\mathbb{E}[Y_{km}])^2}$, where

$$\mathbb{E}\left[Y_{km}\right] = \left(1+\frac{\alpha\ell_k}{N_0 B\beta_m}\right)^{-1}, \tag{32}$$

$$\mathbb{E}\left[Y_{km}^2\right] = \frac{1}{N}\left(\frac{1}{1+\frac{2\alpha\ell_k}{N_0 B\beta_m}}\right) + \frac{N-1}{N}\left(\frac{1}{1+\frac{\alpha\ell_k}{N_0 B\beta_m}}\right)^2. \tag{33}$$

Proof: The proof is given in Appendix F. ■

Result *2:* In the PNEESM method, $\Pr(\mathbf{m}_{\text{opt}} = (m_1, m_2))$ is given by

$$\begin{aligned}\Pr(\mathbf{m}_{\text{opt}} = (m_1, m_2)) \approx{}& \Lambda_{m_1,m_2}(0,0) - \Lambda_{m_1+1,m_2}(0,0) - \Lambda_{m_1,m_2+1}(-u,-1)\\ &- \Lambda_{m_1+v,m_2}(-v,-1) + \Lambda_{m_1+1,m_2+1}(-u-1,-1) + \Lambda_{m_1+v,m_2}(-v+1,-1)\\ &+ \Pi_{m_1+v,m_2+1}(-v-u,-v) - \Pi_{m_1+v,m_2+1}(-v-u,-v+1),\end{aligned} \tag{34}$$

where

$$\Lambda_{m_1,m_2}(x,y) = \sum_{i=1}^{p} w_i f_{m_1,m_2}(q_i) B_i\left(\exp\left(-K^{(1)}_{m_1,m_2}(q_i,x,y)\right), a_{m_1}, b_{m_1}\right), \tag{35}$$

$$\Pi_{m_1,m_2}(x,y) = \sum_{i=1}^{p} w_i f_{m_1,m_2}(q_i) B_i\left(\exp\left(-K^{(2)}_{m_1,m_2}(q_i,x,y)\right), a_{m_1}, b_{m_1}\right). \tag{36}$$

Here, $f_l(z) = \frac{\exp\left(-\frac{a_l\alpha T_l}{\beta_l P}\right)}{a_l B(a_l,b_l)}\left(1-\exp\left(-\frac{z+\frac{a_l\alpha T_l}{\beta_l P}}{a_l}\right)\right)^{b_l-1}$, $Z_l(z) = \frac{\beta_l}{a_l}\left(z+\frac{a_l\alpha T_l}{\beta_l P}\right)$, $K^{(1)}_{m_1,m_2}(z,m,n)$ $\triangleq$ $\frac{1}{\beta_{m_1}}\max\left\{\frac{\alpha T_{m_1} Z_{m_2}(z)(T_{m_2+n}+1)}{Z_{m_2}(z)P-\alpha T_{m_2+n}}, \frac{\alpha T_{m_1+m} Z_{m_2}(z)(T_{m_2}+1)}{Z_{m_2}(z)P-\alpha T_{m_2}}, \frac{2\alpha T_{m_1}}{P}\right\}$, q_i and w_i, for $1 \leq i \leq p$, are the Gauss-quadrature abscissas and weights, respectively [36, Table 25.9], p is the number of terms, and $K^{(2)}_{m_1,m_2}(z,m,n)$ $\triangleq$ $\frac{1}{\beta_{m_1}}\max\left\{\frac{\alpha T_{m_1} Z_{m_2}(z)(T_{m_2-2}+1)}{Z_{m_2}(z)P-\alpha T_{m_2-2}}, \frac{\alpha T_{m_1+m} Z_{m_2}(z)(T_{m_2}+1)}{Z_{m_2}(z)P-\alpha T_{m_2}}, \frac{2\alpha T_{m_1}}{P}, \frac{\alpha T_{m_1+n} Z_{m_2}(z)(T_{m_2-1}+1)}{Z_{m_2}(z)P-\alpha T_{m_2-1}}\right\}$.

Proof: The proof is given in Appendix G. ■

When $v = 0$ and $m_1 \neq L$, the event E_4 is the null event $\emptyset$ and $\Pr(E_1 \cap E_2 \cap E_3 \cap E_4) = \Pr(E_1 \cap E_4) = \Pr(E_1 \cap E_3 \cap E_4) = \Pr(E_1 \cap E_2 \cap E_4) = 0$ in (29). When $m_1 = L$, the events E_2 and E_4 are $\emptyset$ and $\Pr(E_1 \cap E_4) = \Pr(E_1 \cap E_3 \cap E_4) = \Pr(E_1 \cap E_2 \cap E_3 \cap E_4) = 0$. Similarly, for $m_2 = L$, we have $E_3 = \emptyset$ and the probability terms containing E_3 are 0.

IV. Generalization to Multiple Users

We now generalize our approach to $K = 3$ and more users. As before, the users are indexed in the ascending order of their distances from the BS. Therefore, user 1 is the nearest user and user K the farthest. In the SIC-stable regime, user k successively decodes and cancels the signals of users $k+1, \ldots, K$ and then decodes its data.

For $K = 3$ users, we now have the vector of six SINRs $\mathbf{\Gamma}_{kj}$ for $(k,j) \in \{(1,1),(1,2),(1,3),(2,2),(2,3),(3,3)\}$. The definitions of $\gamma_{11}^{(n)}, \gamma_{12}^{(n)}$, and $\gamma_{22}^{(n)}$ are the same as those defined in Section II. The SINR $\gamma_{13}^{(n)}$ of PRB n of the user 1 when it decodes user 3's data is given by $\gamma_{13}^{(n)} = \frac{P_3 \ell_1 g_{1n}}{P_1 \ell_1 g_{1n} + P_2 \ell_1 g_{1n} + N_0 B}$. The SINR $\gamma_{23}^{(n)}$ of PRB n of user 2 when it decodes user 3's data is $\gamma_{23}^{(n)} = \frac{P_3 \ell_2 g_{2n}}{P_1 \ell_2 g_{2n} + P_2 \ell_2 g_{2n} + N_0 B}$. The SINR $\gamma_{33}^{(n)}$ of PRB n of user 3 when it decodes its own data is $\gamma_{33}^{(n)} = \frac{P_3 \ell_3 g_{3n}}{P_1 \ell_3 g_{3n} + P_2 \ell_3 g_{3n} + N_0 B}$.

Let m_3 be the MCS and w_3 be the weight given for user 3. The problem statement using EESM now becomes the following in the SIC-stable regime:

$$\mathcal{S}_1' : \max_{\substack{m_1,m_2,m_3 \in \Omega, \\ P_1 \geq 0, P_2 \geq 0, P_3 \geq 0}} \quad \{r_{m_1} + w_2 r_{m_2} + w_3 r_{m_3}\}, \tag{37}$$

$$\text{s.t.} \quad \tilde{\Gamma}_{11}(m_1) \geq T_{m_1}, \tag{38}$$

$$\min\{\tilde{\Gamma}_{12}(m_2), \tilde{\Gamma}_{22}(m_2)\} \geq T_{m_2}, \tag{39}$$

$$\min\{\tilde{\Gamma}_{13}(m_3), \tilde{\Gamma}_{23}(m_3), \tilde{\Gamma}_{33}(m_3)\} \geq T_{m_3}, \tag{40}$$

$$P_1 + P_2 + P_3 = P, \tag{41}$$

$$P_1 < P_2, \text{ if } m_2 > 0, \text{ and } P_1 + P_2 < \frac{P}{2}, \text{ if } m_3 > 0, \tag{42}$$

with $w_3 \geq w_2 \geq 1$. The constraint in (40) requires that the BLER of user 3's data when decoded by users $1, 2$, and 3, should not exceed ϵ. The total power constraint and the SIC-stable regime constraints are given in (41) and (42), respectively. Since the channel power gain of the user

1 is greater than that of the users 2 and 3 with high probability, we get $\tilde{\Gamma}_{22}(m_2) < \tilde{\Gamma}_{12}(m_2)$ and $\tilde{\Gamma}_{33}(m_3) < \tilde{\Gamma}_{23}(m_3) < \tilde{\Gamma}_{13}(m_3)$. Therefore, (39) simplifies to $\tilde{\Gamma}_{22}(m_2) \geq T_{m_2}$ and (40) simplifies to $\tilde{\Gamma}_{33}(m_3) \geq T_{m_3}$. Compared to $\mathcal{S}_1$, the objective function is different and two additional constraints in (40) and (42) are added. The constraint in (42) is removed for the information-theoretic regime.

To determine whether the MCS triplet (m_1, m_2, m_3) is feasible, the barrier function F' is constructed as follows based on the constraints in (38), (39), (40), and (42):

$$F'(P_1, P_2) = \exp\left(-\left[\tilde{\Gamma}_{11}(m_1) - T_{m_1}\right]\right) + \exp\left(-\left[\tilde{\Gamma}_{22}(m_2) - T_{m_2}\right]\right) + \exp\left(-\left[\tilde{\Gamma}_{33}(m_3) - T_{m_3}\right]\right) + \exp\left(-\left[\frac{P}{2} - P_1 - P_2\right]\right) + \exp\left(-\left[P_2 - P_1\right]\right). \quad (43)$$

For $m_3 = 0$, the fourth term is absent. For $m_2 = 0$, the fifth term is absent. As for $K = 2$, we minimize F' using gradient descent. For the information-theoretic regime, only the first three terms in (43) need to be included in F'.

The following additional lemma, along with Lemmas 2 and 3, enables us to apply PB. It connects $\tilde{\Gamma}_{33}(m_3)$ and $\tilde{G}_3(m_3)$. Let $\overline{\mathsf{SNR}}_k = \frac{P_k \ell_3}{N_0 B N} \sum_{n=1}^{N} g_{3n}$.

Lemma *5:* When β_{m_3} and $\overline{\mathsf{SNR}}_2$ are larger, $\tilde{\Gamma}_{33}(m_3)$ is upper bounded by

$$\tilde{\Gamma}_{33}(m_3) \leq \frac{\frac{P_3}{\alpha}\tilde{G}_3(m_3)}{\frac{P_1}{\alpha}\tilde{G}_3(m_3) + \frac{P_2}{\alpha}\tilde{G}_3(m_3) + 1} + \frac{P_3}{P_1 + P_2}\mathcal{O}\left(\frac{1}{\overline{\mathsf{SNR}}_1 + \overline{\mathsf{SNR}}_2}\right). \quad (44)$$

When $\overline{\mathsf{SNR}}_2$ is small and $\frac{P_3}{\alpha} \geq 1$, $\tilde{\Gamma}_{33}(m_3)$ is upper bounded by

$$\tilde{\Gamma}_{33}(m_3) \leq \frac{\frac{P_3}{\alpha}\tilde{G}_3(m_3)}{\frac{P_1}{\alpha}\tilde{G}_3(m_3) + \frac{P_2}{\alpha}\tilde{G}_3(m_3) + 1}. \quad (45)$$

Proof: The proof is given in Appendix E. ■

Similar to Figure 2, we numerically find that Lemma 5 holds with high probability for all values of interest of β_{m_3} and powers.

We then replace the inequalities in (38), (39), and (40) with their upper bounds based on PNEESM. It yields an optimization problem similar to $\mathcal{S}_2$, which is linear in the powers and is a relaxation of $\mathcal{S}_1'$ when Lemmas 2, 3, and 5 hold. It leads to the following closed-form test for the feasibility of an MCS triplet (m_1, m_2, m_3).

Result *3:* For an MCS triplet (m_1, m_2, m_3), a feasible power allocation for the PNEESM method $\mathcal{S}_2'$ exists if and only if

$$\max\left\{\frac{\alpha T_{m_1}}{\tilde{G}_1(m_1)}, K_1\right\} < \min\left\{\frac{K_3 + \frac{P}{2} - K_2}{1 + T_{m_3}}, K_3\right\}, \tag{46}$$

where $K_1 = \frac{T_{m_2}\left(\alpha T_{m_1}\tilde{G}_2(m_2) + \alpha\tilde{G}_1(m_1)\right)}{\tilde{G}_1(m_1)\tilde{G}_2(m_2)}$, $K_2 = \frac{T_{m_3}\left(\alpha T_{m_1}\tilde{G}_3(m_3) + \alpha\tilde{G}_1(m_1)\right)}{\tilde{G}_1(m_1)\tilde{G}_3(m_3)}$, and $K_3 = \frac{P}{2} - \frac{\alpha T_{m_1}}{\tilde{G}_1(m_1)}$.

Proof: The proof is similar to Appendix D and is skipped. ■

For the information-theoretic regime, the corresponding result is given by $K_1 < \frac{K_3 + \frac{P}{2} - K_2}{1 + T_{m_3}}$. Therefore, no numerical search is needed to assess the feasibility of an MCS triplet. PB can then be easily extended to the three-user case. We skip the details to conserve space.

In general, for K users, the effective SINR $\tilde{\Gamma}_{kk}(m_k)$ can be upper bounded in terms of $\tilde{G}_k(m_k)$ as

$$\tilde{\Gamma}_{kk}(m_k) \leq \frac{\frac{P_k}{\alpha}\tilde{G}_k(m_k)}{(P_1 + P_2 + \cdots + P_{k-1})\frac{\tilde{G}_k(m_k)}{\alpha} + 1} + \frac{P_k}{P_1 + P_2 + \cdots + P_{k-1}}\mathcal{O}\left(\frac{1}{\overline{\mathsf{SNR}}_1 + \overline{\mathsf{SNR}}_2 + \cdots + \overline{\mathsf{SNR}}_{k-1}}\right), \tag{47}$$

when β_{m_k} and $\overline{\mathsf{SNR}}_{k-1}$ are large. When $\overline{\mathsf{SNR}}_{k-1}$ is small and $\frac{P_k}{\alpha} \geq 1$, $\tilde{\Gamma}_{kk}$ can be bounded as

$$\tilde{\Gamma}_{kk}(m_k) \leq \frac{\frac{P_k}{\alpha}\tilde{G}_k(m_k)}{(P_1 + P_2 + \cdots + P_{k-1})\frac{\tilde{G}_k(m_k)}{\alpha} + 1}. \tag{48}$$

Therefore along lines similar to $\mathcal{S}_1'$, the BLER constraints can be linearized and feasible solutions found using PB.

V. Numerical Results

We now present Monte Carlo simulation results to characterize the weighted sum rate of wideband NOMA. We set $N = 15$, $\epsilon = 0.1$, $B = 15$ kHz, and $\alpha = 1$. For $K = 2$, we set $w_2 = 4$, and for $K = 3$, we set $w_2 = 5$ and $w_3 = 10$. The BS has 16 MCSs available to it, as specified in [6, Table 5.2.2.1-2]. Their rates range from 0.15 to 5.55 bits/symbol. The results are averaged over 1000 independent realizations of the PRB channel gains of the users.

Figure 3 plots the average weighted sum rate in bits/symbol of wideband NOMA using PB and the effective SINR-based approach as a function of $\frac{P\ell_1}{N_0 B}$, which we shall refer to as the full-power average SNR of the near user. It shows results for the SIC-stable regime for three values

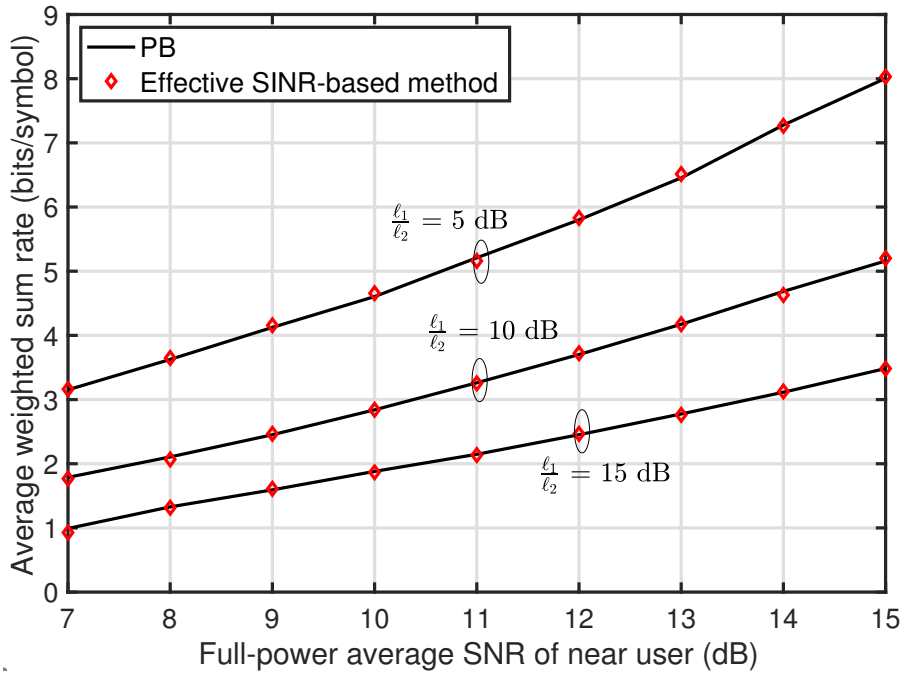

Fig. 3. $K = 2$ users: Average weighted sum rate of wideband NOMA using PB and the effective SINR-based approach as a function of the full-power average SNR of the near user, $\frac{P\ell_1}{N_0 B}$ (SIC-stable regime).

of $\frac{\ell_1}{\ell_2}$. The average weighted sum rate of PB is indistinguishable from that of the effective SINR-based approach for all SNRs and $\frac{\ell_1}{\ell_2}$. Unlike the effective SINR-based method that requires 256 numerical searches, PB requires on average 1.9 and 10.3 feasibility checks for $\frac{P\ell_1}{N_0 B} = 7$ dB and 15 dB, respectively. As $\frac{\ell_1}{\ell_2}$ increases and the near user's average SNR is kept fixed, the average weighted sum rate decreases because the far user's average SNR decreases. The corresponding curves for $K = 3$ are qualitatively similar and are skipped due to space constraints. We henceforth show results for the PB approach.

Figure 4 plots the total average weighted sum rate in bits/frame over the N PRBs of wideband NOMA and wideband OMA as a function of N. It does so for $\frac{\ell_1}{\ell_2} = 5$ dB and 10 dB and the SIC-stable regime. In wideband OMA, the BS transmits to only one user and uses the same MCS and power for all the PRBs, as required by the standard. As N increases, the total average weighted sum rate increases, but sub-linearly. This is because rate and power adaptation on a per-PRB basis are not allowed. We note that $N = 1$ is equivalent to the flat-fading and per-PRB adaptation models studied in the literature [7]–[10]. Since the increase in total average weighted

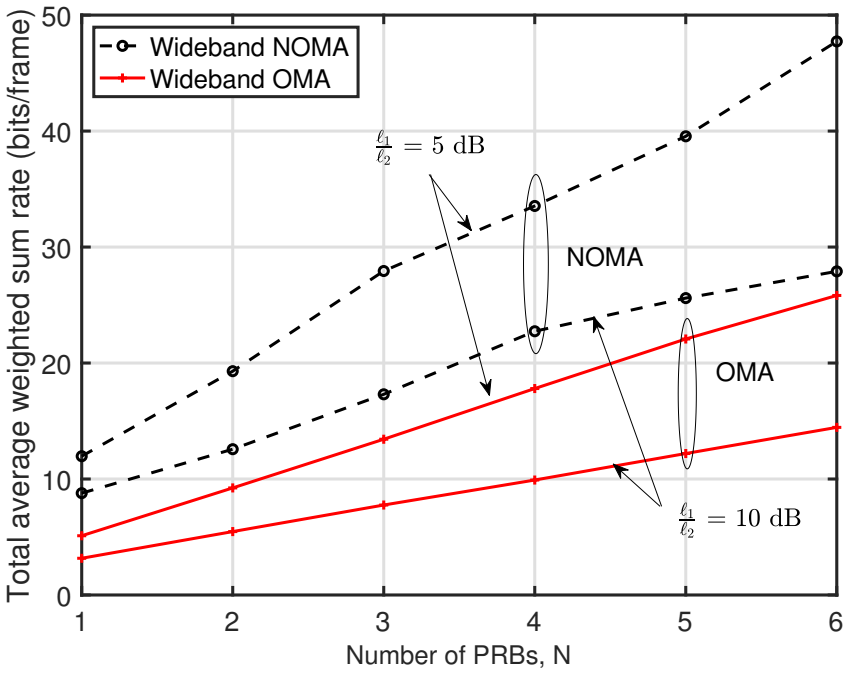

Fig. 4. Comparison of total average weighted sum rates of wideband NOMA and wideband OMA as a function of the number of PRBs for two values of $\frac{\ell_1}{\ell_2}$ (SIC-stable regime, $K = 2$, and $\frac{P\ell_1}{N_0 B} = 15$ dB).

sum rate is not linear, these models overestimate the average weighted sum rate. Furthermore, wideband NOMA achieves a substantially higher average weighted sum rate than wideband OMA for all values of N and $\frac{\ell_1}{\ell_2}$.

Figure 5 benchmarks the average weighted sum rate in bits/symbol of wideband NOMA with continuous rate adaptation [12]–[15], [18]–[21], [27], OMA with discrete rate adaptation, dynamic power and rate adaptation (DPRA) [11], and our proposed method. In DPRA, the far user is first assigned its minimum rate and the least power required to support it. Then, the near user's rate is chosen to be as large as possible with the remaining power. Thereafter, the far user's rate is increased if any power is still left. As $\frac{\ell_1}{\ell_2}$ increases, the average weighted sum rate decreases for all the schemes. This is because of the reduction in the far user's SNR by keeping the near user's SNR fixed. We see that continuous rate adaptation overestimates the average weighted sum rate achieved by discrete rate adaptation, which is used in practice. Wideband NOMA outperforms DPRA and OMA.

Figure 6 plots results from analysis and simulations for the average weighted sum rate of the

This article has been accepted for publication in IEEE Transactions on Wireless Communications. This is the author's version which has not been fully edited and content may change prior to final publication. Citation information: DOI 10.1109/TWC.2023.3315709

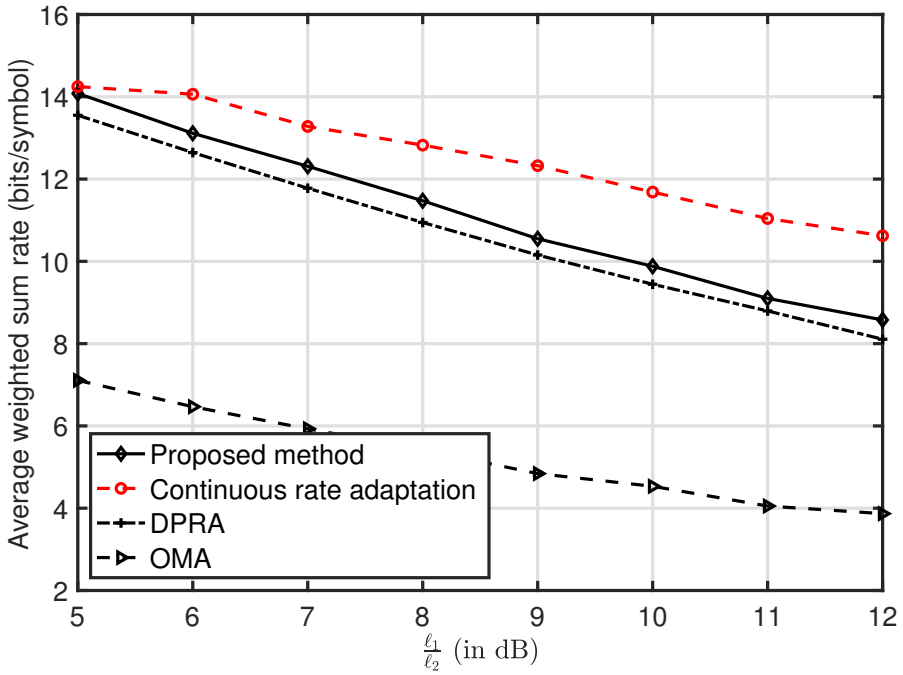

Fig. 5. $K = 2$ users: Benchmarking of average weighted sum rate as a function of $\frac{\ell_1}{\ell_2}$ for $N = 1$ (SIC-stable regime and $\frac{P\ell_1}{N_0 B} = 20$ dB).

PNEESM method (cf. Section III-C) for $N = 15$ and $K = 2$. It also compares them with the average weighted sum rate of PB, which employs an additional backtracking step. The PNEESM method overestimates the average weighted sum rate given that it is a relaxation. The analysis tracks the simulation results well and is exact at larger average SNRs.

Figure 7 shows results for $K = 3$. It plots the average weighted sum rate for the SIC-stable and information-theoretic regimes as a function of the full-power average SNR of user 1. The average weighted sum rate with the information-theoretic regime is greater than that with the SIC-stable regime since the latter imposes an extra constraint (cf. (42)). However, the gap between the two is small. Thus, the SIC-stable regime, which makes the receiver implementation easier, can be used in practice with a negligible loss in performance. The behavior for $K = 2$ is qualitatively similar and is not shown.

This article has been accepted for publication in IEEE Transactions on Wireless Communications. This is the author's version which has not been fully edited and content may change prior to final publication. Citation information: DOI 10.1109/TWC.2023.3315709

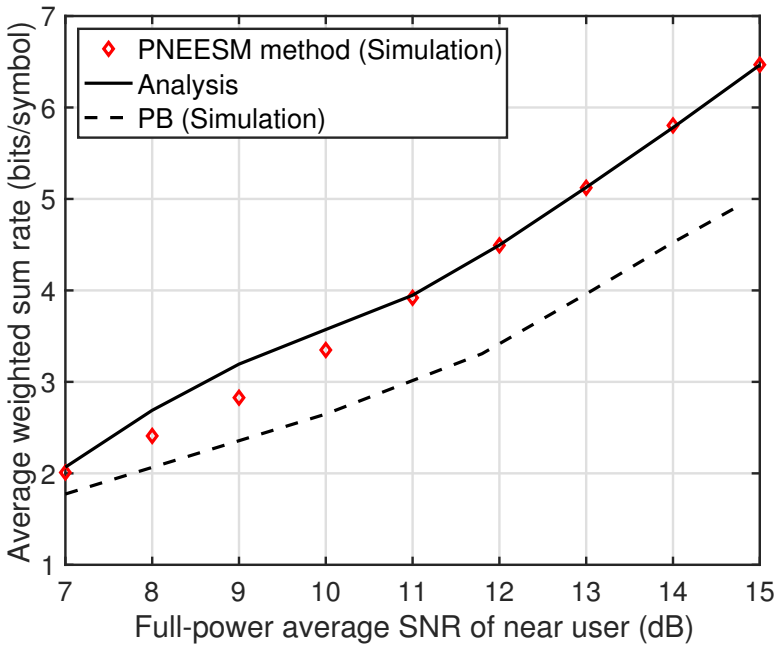

Fig. 6. Zoomed-in comparison of the average weighted sum rates of the PNEESM method (analysis and simulations) and PB ($\frac{\ell_1}{\ell_2} = 10$ dB, $K = 2$, and SIC-stable regime).

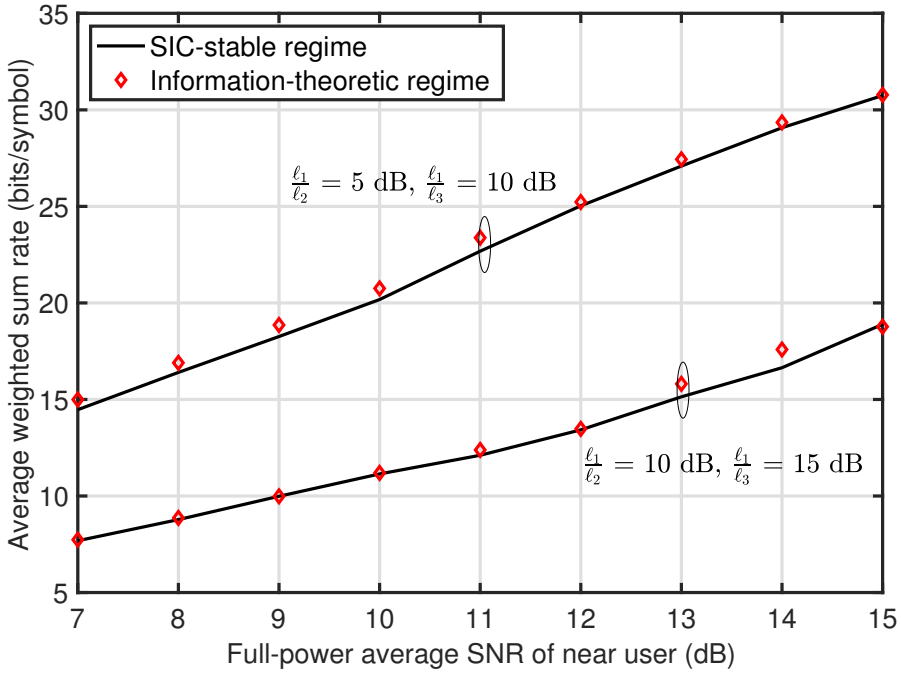

Fig. 7. $K = 3$ users: Zoomed in comparison of the average weighted sum rates with the SIC-stable and information-theoretic regimes for different pathloss ratios.

VI. Conclusions

The common discrete MCS and power constraint, which helps to limit the control and feedback signaling overhead in an OFDM-based cellular system, requires a new approach to determine the MCSs and powers of wideband NOMA. We presented a novel approach based on effective SINRs for multiple users wideband NOMA. We also presented PB, which exploited the properties of PNEESM to lower the complexity. PNEESM enabled the non-linear constraints in the users' powers imposed by EESM to be replaced with linear constraints. We showed that this led to a relaxation of the original optimization problem under various conditions on the subcarrier-averaged SNRs of the users and the MCS-dependent scaling constant.

The average weighted sum rate of PB was indistinguishable from that of the effective SINR-based approach. Wideband NOMA had a higher average weighted sum rate than wideband OMA, which is currently employed by 5G NR, and other algorithms considered in the literature. The difference in performance between the SIC-stable and information-theoretic regimes was negligible. We also saw that the per-PRB and continuous rate adaptation models overestimated the average weighted sum rate. An interesting avenue for future work is wideband NOMA for multi-user and multi-cell multiple-input-multiple-output (MIMO) systems. In these systems, the effective SINRs of the users now depend on the inter-cell and inter-layer interferences.

Appendix

A. *Proof of Lemma 1*

To prove that PNEESM $\tilde{G}_k(m)$ is an increasing function of m, it is sufficient to show that $\tilde{G}_k(m)$ increases as β_m increases because $\beta_m < \beta_{m+1}$. From (14), $\frac{d\tilde{G}_k(m)}{d\beta_m}$ is given by

$$\begin{aligned}\frac{d\tilde{G}_k(m)}{d\beta_m} &= -\ln\left(\frac{1}{N}\sum_{n=1}^{N}\exp\left[-\frac{\alpha\ell_k g_{kn}}{N_0 B\beta_m}\right]\right) - \frac{\alpha\ell_k}{N_0 B\beta_m}\sum_{n=1}^{N}\frac{g_{kn}\exp\left(-\frac{\alpha\ell_k g_{kn}}{N_0 B\beta_m}\right)}{\sum_{n=1}^{N}\exp\left(-\frac{\alpha\ell_k g_{kn}}{N_0 B\beta_m}\right)},\\ &= \ln(N) - \sum_{n=1}^{N} v_n \ln(v_n), \end{aligned} \tag{49}$$

where $v_n = \frac{\exp\left(-\frac{\alpha\ell_k g_{kn}}{N_0 B\beta_m}\right)}{\sum_{n=1}^{N}\exp\left(-\frac{\alpha\ell_k g_{kn}}{N_0 B\beta_m}\right)}$. Note that v_n lies between 0 and 1, and $\sum_{n=1}^{N} v_n = 1$. Thus, $\{v_n\}_{n=1}^{N}$ is a probability mass function. From Jensen's inequality, it follows that $\sum_{n=1}^{N} v_n \ln(v_n) \leq \ln(N)$. Thus, $\frac{d\tilde{G}_k(m)}{d\beta_m} \geq 0$.

B. Proof of Lemma 2

We know that $\exp\left(-\frac{P_2\ell_2 g_{2n}}{(P_1\ell_2 g_{2n}+N_0B)\beta_{m_2}}\right) > \exp\left(\frac{-P_2}{P_1\beta_{m_2}}\right)$. Summing over n from 1 to N on both sides, we get $\frac{1}{N}\sum_{n=1}^{N}\exp\left(-\frac{P_2\ell_2 g_{2n}}{(P_1\ell_2 g_{2n}+N_0B)\beta_{m_2}}\right) > \exp\left(\frac{-P_2}{P_1\beta_{m_2}}\right)$. Taking logarithm on both sides and rearranging the terms, we get

$$\tilde{\Gamma}_{22}\left(m_2\right) < \frac{P_2}{P_1}. \tag{50}$$

As $\beta_{m_2}\to\infty$, using the L'Hôpital's rule, the right hand side of (15) simplifies to

$$\lim_{\beta_{m_2}\to\infty}\frac{\frac{P_2}{\alpha}\tilde{G}_2\left(m_2\right)}{\frac{P_1}{\alpha}\tilde{G}_2\left(m_2\right)+1} = \frac{\frac{P_2}{\alpha}\frac{1}{N}\sum_{n=1}^{N}\frac{\alpha\ell_2 g_{2n}}{N_0B}}{\frac{P_1}{\alpha}\frac{1}{N}\sum_{n=1}^{N}\frac{\alpha\ell_2 g_{2n}}{N_0B}+1} = \frac{\overline{\mathsf{SNR}}_2}{\overline{\mathsf{SNR}}_1+1}, \tag{51}$$

where $\overline{\mathsf{SNR}}_k = \frac{P_k\ell_2}{N_0BN}\sum_{n=1}^{N} g_{2n}$. For large $\overline{\mathsf{SNR}}_1$, we have $\frac{\overline{\mathsf{SNR}}_2}{\overline{\mathsf{SNR}}_1+1} = \frac{P_2}{P_1}\left(1-\mathcal{O}\left(\frac{1}{\overline{\mathsf{SNR}}_1}\right)\right)$ since $\frac{\overline{\mathsf{SNR}}_2}{\overline{\mathsf{SNR}}_1} = \frac{P_2}{P_1}$. Hence,

$$\lim_{\beta_{m_2}\to\infty}\frac{\frac{P_2}{\alpha}\tilde{G}_2\left(m_2\right)}{\frac{P_1}{\alpha}\tilde{G}_2\left(m_2\right)+1} = \frac{P_2}{P_1}\left[1-\mathcal{O}\left(\frac{1}{\overline{\mathsf{SNR}}_1}\right)\right]. \tag{52}$$

Combining (50) and (52) yields (15).

For small $\overline{\mathsf{SNR}}_1$, $P_1\ell_2 g_{2n} \ll N_0B$. Hence, the effective SINR $\tilde{\Gamma}_{22}\left(m_2\right)$ using (7) simplifies to

$$\tilde{\Gamma}_{22}\left(m_2\right) = -\beta_{m_2}\ln\left(\frac{1}{N}\sum_{n=1}^{N}\exp\left[-\frac{P_2\ell_2 g_{2n}}{N_0B\beta_{m_2}}\right]\right). \tag{53}$$

Similar to Lemma 1, we can show that EESM is a monotonically increasing function of β_{m_2}. Since $\frac{\alpha\beta_{m_2}}{P_2} \le \beta_{m_2}$ for $\frac{P_2}{\alpha}\ge 1$, it follows that

$$\tilde{\Gamma}_{22}\left(m_2\right) = -\frac{P_2}{\alpha}\frac{\beta_{m_2}\alpha}{P_2}\ln\left(\frac{1}{N}\sum_{n=1}^{N}\exp\left[-\frac{\alpha\ell_2 g_{2n}}{N_0B\frac{\beta_{m_2}\alpha}{P_2}}\right]\right) \le \frac{P_2}{\alpha}\tilde{G}_2\left(m_2\right). \tag{54}$$

For small $\overline{\mathsf{SNR}}_1$, we have $\frac{P_1}{\alpha}\tilde{G}_2\left(m_2\right) \ll 1$, which implies that $\frac{\frac{P_2}{\alpha}\tilde{G}_2(m_2)}{\frac{P_1}{\alpha}\tilde{G}_2(m_2)+1\approx 1} \approx \frac{P_2}{\alpha}\tilde{G}_2\left(m_2\right)$. Hence, (16) follows.

C. Proof of Lemma 3

The effective SINR $\tilde{\Gamma}_{11}\left(m_1\right)$ in (7) can be rewritten as follows:

$$\tilde{\Gamma}_{11}\left(m_1\right) = -\frac{P_1}{\alpha}\frac{\beta_{m_1}\alpha}{P_1}\ln\left(\frac{1}{N}\sum_{n=1}^{N}\exp\left[-\frac{\alpha\ell_1 g_{1n}}{N_0B\frac{\beta_{m_1}\alpha}{P_1}}\right]\right) = \frac{P_1}{\alpha}\mathsf{EESM}\left(\frac{\alpha\ell_1\mathbf{g}_1}{N_0B},\frac{\beta_{m_1}\alpha}{P_1}\right). \tag{55}$$

As above, the EESM is an increasing function of β_{m_1}. Hence, for $\frac{P_1}{\alpha}\ge 1$, $\mathsf{EESM}\left(\frac{\alpha\ell_1\mathbf{g}_1}{N_0B},\frac{\beta_{m_1}\alpha}{P_1}\right) \le \mathsf{EESM}\left(\frac{\alpha\ell_1\mathbf{g}_1}{N_0B},\beta_{m_1}\right) = \tilde{G}_1\left(m_1\right)$. Therefore, $\tilde{\Gamma}_{11}\left(m_1\right) \le \frac{P_1}{\alpha}\tilde{G}_1\left(m_1\right)$.

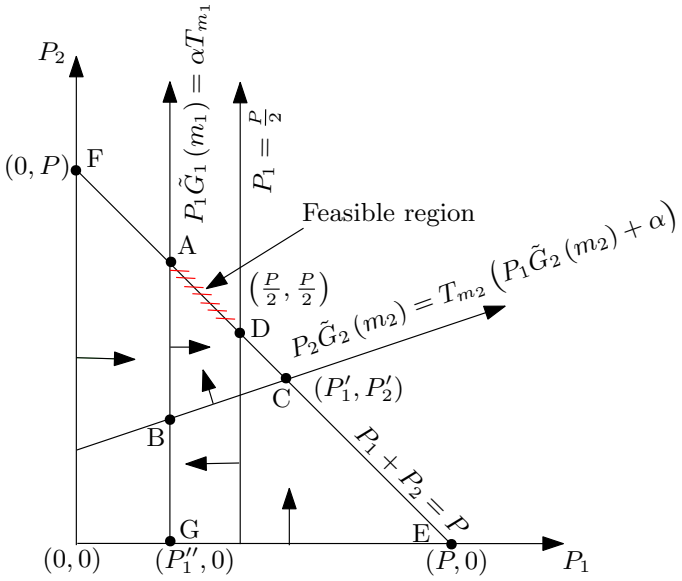

Fig. 8. Illustration of the feasible region for power allocation for MCS pair (m_1, m_2) using the PNEESM method.

D. Proof of Result 1

The constraints in (19), (20), and (22) are illustrated in Figure 8. The arrows represent the feasible region for each constraint. The shaded line segment shows the feasible region for the constraint in (21). A feasible (P_1, P_2) that satisfies all the constraints exists if both vertices C and D are to the right of the vertical line that joins A and B. The x co-ordinate of A and B, which we denote by P_1'', is obtained by replacing the inequality in (19) with an equality. It is given by $P_1'' = \frac{\alpha T_{m_1}}{\tilde{G}_1(m_1)}$. Let (P_1', P_2') be the co-ordinates of C, which is the intersection of the boundary lines of the regions defined by the inequalities in (20) and (21). We can show that $P_1' = \frac{\tilde{G}_2(m_2)P - \alpha T_{m_2}}{\tilde{G}_2(m_2)\left(T_{m_2}+1\right)}$. Hence, a feasible (P_1, P_2) exists if and only if $P_1'' \leq P_1'$ and $P_1'' < \frac{P}{2}$. These two conditions yield (24).

Notice that (P_1, P_2) need not be unique. This is an outcome of discrete rate adaptation, and is different from continuous rate adaptation [7], [12].

E. Proof of Lemma 5

We know that $\exp\left(-\frac{P_3\ell_3 g_{3n}}{(P_1\ell_3 g_{3n}+P_2\ell_3 g_{3n}+N_0B)\beta_{m_3}}\right) > \exp\left(\frac{-P_3}{(P_1+P_2)\beta_{m_3}}\right)$. Along lines similar to Lemma 2, summing over n from 1 to N and taking logarithm on both sides, we get

$$\tilde{\Gamma}_{33}\left(m_3\right) < \frac{P_3}{P_1+P_2}. \tag{56}$$

As $\beta_{m_3} \to \infty$ and for higher $\overline{\mathsf{SNR}}_2$, we get the following:

$$\lim_{\beta_{m_3}\to\infty} \frac{\frac{P_3}{\alpha}\tilde{G}_3\left(m_3\right)}{\frac{P_1}{\alpha}\tilde{G}_3\left(m_3\right)+\frac{P_2}{\alpha}\tilde{G}_3\left(m_3\right)+1} = \frac{P_3}{P_1+P_2}\left(1-\mathcal{O}\left(\frac{1}{\overline{\mathsf{SNR}}_1+\overline{\mathsf{SNR}}_2}\right)\right). \tag{57}$$

Combining (56) and (57) yields (44).

For small $\overline{\mathsf{SNR}}_2$, $P_1\ell_3 g_{3n} + P_2\ell_3 g_{3n} \ll N_0B$ since $P_1 < P_2$. Hence, the effective SINR $\tilde{\Gamma}_{33}\left(m_3\right)$ simplifies to

$$\tilde{\Gamma}_{33}\left(m_3\right) = -\beta_{m_3}\ln\left(\frac{1}{N}\sum_{n=1}^{N}\exp\left(-\frac{P_3\ell_3 g_{3n}}{N_0B\beta_{m_3}}\right)\right) = \frac{P_3}{\alpha}\mathsf{EESM}\left(\frac{\alpha\ell_3\mathbf{g}_3}{N_0B}, \frac{\alpha\beta_{m_3}}{P_3}\right). \tag{58}$$

Since $\mathsf{EESM}\left(\frac{\alpha\ell_3\mathbf{g}_3}{N_0B}, \frac{\alpha\beta_{m_3}}{P_3}\right) \leq \mathsf{EESM}\left(\frac{\alpha\ell_3\mathbf{g}_3}{N_0B}, \beta_{m_3}\right) = \tilde{G}_3\left(m_3\right)$ for $\frac{P_3}{\alpha} \geq 1$, the above equation implies that $\tilde{\Gamma}_{33}\left(m_3\right) \leq \frac{P_3}{\alpha}\tilde{G}_3\left(m_3\right)$.

For small $\overline{\mathsf{SNR}}_2$, as above, we get $\frac{P_1}{\alpha}\tilde{G}_3\left(m_3\right)+\frac{P_2}{\alpha}\tilde{G}_3\left(m_3\right) \ll 1$, which implies that $\frac{P_3}{\alpha}\tilde{G}_3\left(m_3\right) \approx \frac{\frac{P_3}{\alpha}\tilde{G}_3(m_3)}{\frac{P_1}{\alpha}\tilde{G}_3(m_3)+\frac{P_2}{\alpha}\tilde{G}_3(m_3)+1}$. Hence, (45) follows.

F. Statistics of $\tilde{G}_k(m)$

Let $Y_{km} = \frac{1}{N}\sum_{n=1}^{N}\exp\left(-\frac{\alpha g_{kn}\ell_k}{N_0B\beta_m}\right)$ denote the term inside the logarithm in (14), for $k \in \{1,2\}$. It lies between 0 and 1. Motivated by Papoulis' central limit approximation, Y_{km} can be approximated as a Beta RV with parameters a_m and b_m [28]. Hence, the CDF of $\tilde{G}_k(m)$ is

$$\begin{aligned} F_{\tilde{G}_k(m)}\left(x\right) = \Pr\left(-\beta_m\ln(Y_{km}) \leq x\right) &= \Pr\left(Y_{km} \geq \exp\left(-\frac{x}{\beta_m}\right)\right), \\ &= 1 - B_i\left(\exp\left(-\frac{x}{\beta_m}\right), a_m, b_m\right), \text{ for } x \geq 0. \end{aligned} \tag{59}$$

Differentiating (59) with respect to x yields the PDF in (31).

The parameters a_m and b_m can be expressed in terms of the first and second moments of Y_{km} as per (32) and (33) [28]. The first and second moments of Y_{km} can, in turn, be expressed in

terms of the system parameters as follows. Since $g_{k1}, \ldots, g_{kN}$ are independent and identically distributed exponential RVs with unit mean, we get

$$\mathbb{E}\left[Y_{km}\right] = \mathbb{E}\left[\exp\left(\frac{-\alpha \ell_k g_{k1}}{N_0 B \beta_m}\right)\right] = \left(1 + \frac{\alpha \ell_k}{N_0 B \beta_m}\right)^{-1}. \tag{60}$$

Similarly, taking expectation over Y_{km}^2 and simplifying, we get

$$\begin{aligned}\mathbb{E}\left[Y_{km}^2\right] &= \frac{1}{N^2}\left(\sum_{i=1}^{N}\mathbb{E}\left[\exp\left(\frac{-2\alpha \ell_k g_{ki}}{N_0 B \beta_m}\right)\right] + \sum_{i=1}^{N}\sum_{j=1, j\neq i}^{N}\mathbb{E}\left[\exp\left(\frac{-\alpha \ell_k g_{ki}}{N_0 B \beta_m}\right)\exp\left(\frac{-\alpha \ell_k g_{kj}}{N_0 B \beta_m}\right)\right]\right), \\ &= \frac{1}{N}\left(\frac{1}{1 + \frac{2\alpha \ell_k}{N_0 B \beta_m}} + \frac{N-1}{\left(1 + \frac{\alpha \ell_k}{N_0 B \beta_m}\right)^2}\right). \end{aligned} \tag{61}$$

G. Derivation of Result 2

We evaluate the different probability terms in (29) separately below.

a) Evaluation of Pr (E_1): Applying Result 1 to the MCS pair (m_1, m_2), we get

$$\Pr\left(E_1\right) = \Pr\left(\tilde{G}_1(m_1) > \max\left\{\frac{\alpha T_{m_1}\tilde{G}_2(m_2)(T_{m_2}+1)}{\tilde{G}_2(m_2)P - \alpha T_{m_2}}, \frac{2\alpha T_{m_1}}{P}\right\}, \tilde{G}_2(m_2) \geq \frac{\alpha T_{m_2}}{P}\right). \tag{62}$$

Conditioning on $\tilde{G}_2(m_2)$, we get

$$\Pr\left(E_1\right) = \mathbb{E}\left[\Pr\left(\tilde{G}_1(m_1) > k_{m_1,m_2}(x, m_1, m_2), x \geq \frac{\alpha T_{m_2}}{P} \;\middle|\; \tilde{G}_2(m_2) = x\right)\right], \tag{63}$$

where $k_{m_1,m_2}(x, c, d) \triangleq \max\left\{\frac{\alpha T_{m_1} x(T_d+1)}{xP - \alpha T_d}, \frac{\alpha T_{m_2} x(T_c+1)}{xP - \alpha T_c}, \frac{2\alpha T_{m_1}}{P}\right\}$. Writing this in terms of the CDF of $\tilde{G}_1(m_1)$ and the PDF of $\tilde{G}_2(m_2)$, we get

$$\Pr\left(E_1\right) = \int_{\frac{\alpha T_{m_2}}{P}}^{\infty}\left(1 - F_{\tilde{G}_1(m_1)}\left(k_{m_1,m_2}(x, m_1, m_2)\right)\right) f_{\tilde{G}_2(m_2)}\left(x\right)\, dx. \tag{64}$$

Substituting in (64) the CDF in (59) for $\tilde{G}_1(m_1)$ and the PDF in (31) for $\tilde{G}_2(m_2)$, we get

$$\begin{aligned}\Pr\left(E_1\right) = \int_{0}^{\infty} &\exp(-x)\exp\left(-\frac{a_{m_2}\alpha T_{m_2}}{\beta_{m_2} P}\right)\left(1 - \exp\left[-\frac{x + \frac{a_{m_2}\alpha T_{m_2}}{\beta_{m_2} P}}{a_{m_2}}\right]\right)^{b_{m_2}-1} \\ &\times \frac{B_i\left(\exp\left[-K^{(1)}_{m_1,m_2}(x,0,0)\right], a_{m_1}, b_{m_1}\right)}{a_{m_2} B(a_{m_2}, b_{m_2})}\, dx, \end{aligned} \tag{65}$$

$$= \Lambda_{m_1,m_2}(0,0), \tag{66}$$

where $K^{(1)}_{m_1,m_2}(z,m,n) \triangleq \frac{1}{\beta_{m_1}} \max\left\{\frac{\alpha T_{m_1} Z_{m_2}(z)(T_{m_2+n}+1)}{Z_{m_2}(z)P-\alpha T_{m_2+n}}, \frac{\alpha T_{m_1+m} Z_{m_2}(z)(T_{m_2}+1)}{Z_{m_2}(z)P-\alpha T_{m_2}}, \frac{2\alpha T_{m_1}}{P}\right\}$ and $Z_l(z) = \frac{\beta_l}{a_l}\left(z + \frac{a_l \alpha T_l}{\beta_l P}\right)$. The function $\Lambda_{m_1,m_2}(0,0)$ can be evaluated using Gauss-Laguerre quadrature with p terms as follows [36]:

$$\Lambda_{m_1,m_2}(0,0) \approx \sum_{i=1}^{p} \frac{w_i \exp\left(-\frac{a_{m_2}\alpha T_{m_2}}{\beta_{m_2}P}\right)}{a_{m_2} B(a_{m_2}, b_{m_2})} \left(1 - \exp\left[-\frac{q_i + \frac{a_{m_2}\alpha T_{m_2}}{\beta_{m_2}P}}{a_{m_2}}\right]\right)^{b_{m_2}-1} \times B_i\left(\exp\left(-K^{(1)}_{m_1,m_2}(q_i,0,0)\right), a_{m_1}, b_{m_1}\right), \quad (67)$$

where q_i and w_i, for $1 \le i \le p$, are the abscissas and weights, respectively [36, Table 25.9].

b) Evaluation of Pr $(E_1 \cap E_2)$: From Lemma 1, the PNEESMs of users 1 and 2 increase as the MCS index increases: $\tilde{G}_1(1) < \cdots < \tilde{G}_1(m_1) < \tilde{G}_1(m_1+1) < \cdots < \tilde{G}_1(L)$, and $\tilde{G}_2(1) < \cdots < \tilde{G}_2(m_2) < \tilde{G}_2(m_2+1) < \cdots < \tilde{G}_2(L)$. Using $\tilde{G}_1(m_1) < \tilde{G}_1(m_1+1)$ and applying Result 1 to the MCS pairs (m_1, m_2) and (m_1+1, m_2), we get

$$\Pr(E_1 \cap E_2) = \Pr\left(\tilde{G}_1(m_1+1) > \max\left\{\frac{\alpha T_{m_1+1}\tilde{G}_2(m_2)(T_{m_2}+1)}{\tilde{G}_2(m_2)P - \alpha T_{m_2}}, \frac{2\alpha T_{m_1+1}}{P}\right\}, \tilde{G}_2(m_2) \ge \frac{\alpha T_{m_2}}{P}\right) = \Pr(E_2). \quad (68)$$

$\Pr(E_2)$ is given by replacing m_1 with m_1+1 in (66).

c) Evaluation of Pr $(E_1 \cap E_3)$: Applying Result 1 to the MCS pairs (m_1, m_2) and $(m_1 - u, m_2+1)$, we get

$$\Pr(E_1 \cap E_3) = \Pr\left(\tilde{G}_1(m_1) > \max\left\{\frac{\alpha T_{m_1}\tilde{G}_2(m_2)(T_{m_2}+1)}{\tilde{G}_2(m_2)P - \alpha T_{m_2}}, \frac{2\alpha T_{m_1}}{P}\right\}, \tilde{G}_2(m_2) \ge \frac{\alpha T_{m_2}}{P}, \tilde{G}_1(m_1-u) > \max\left\{\frac{\alpha T_{m_1-u}\tilde{G}_2(m_2+1)(T_{m_2+1}+1)}{\tilde{G}_2(m_2+1)P - \alpha T_{m_2+1}}, \frac{2\alpha T_{m_1-u}}{P}\right\}, \tilde{G}_2(m_2+1) \ge \frac{\alpha T_{m_2+1}}{P}\right). \quad (69)$$

Evaluating the above probability requires the joint distributions of the four correlated RVs $\tilde{G}_1(m_1), \tilde{G}_1(m_1-u), \tilde{G}_2(m_2)$, and $\tilde{G}_2(m_2+1)$, which is intractable. However, in narrowband channels, $\tilde{G}_1(m_1) = \tilde{G}_1(m_1-u)$ and $\tilde{G}_2(m_2) = \tilde{G}_2(m_2+1)$. Hence, in effect, there are only two

RVs. Motivated by this fact, we replace $\tilde{G}_1(m_1-u)$ by $\tilde{G}_1(m_1)$ and $\tilde{G}_2(m_2)$ with $\tilde{G}_2(m_2+1)$. Since $T_{m_1-u} < T_{m_1}$, we get

$$\Pr\left(E_1 \cap E_3\right) \approx \Pr\Bigg(\tilde{G}_2(m_2+1) \geq \frac{\alpha T_{m_2+1}}{P}, \\ \tilde{G}_1(m_1) > \max\left\{\frac{\alpha T_{m_1}\tilde{G}_2(m_2+1)(T_{m_2}+1)}{\tilde{G}_2(m_2+1)P - \alpha T_{m_2}}, \frac{2\alpha T_{m_1}}{P}, \frac{\alpha T_{m_1-u}\tilde{G}_2(m_2+1)(T_{m_2+1}+1)}{\tilde{G}_2(m_2+1)P - \alpha T_{m_2+1}}\right\}\Bigg).$$

Conditioning on $\tilde{G}_2(m_2+1)$, we get

$$\Pr\left(E_1 \cap E_3\right) = \mathbb{E}\left[\Pr\left(\tilde{G}_1(m_1) > k_{m_1,m_2+1}(x, m_1-u, m_2), x \geq \frac{\alpha T_{m_2+1}}{P} \,\middle|\, \tilde{G}_2(m_2+1) = x\right)\right]. \tag{70}$$

This is similar to (63). As above, we can show that $\Pr\left(E_1 \cap E_3\right) = \Lambda_{m_1,m_2+1}(-u,-1)$.

d) Evaluation of Other Probabilities: Along similar lines, we can show the following:

$$\Pr\left(E_1 \cap E_4\right) = \Lambda_{m_1+v,m_2}(-v,-1), \tag{71}$$

$$\Pr\left(E_1 \cap E_2 \cap E_3\right) = \Pr\left(E_2 \cap E_3\right) = \Lambda_{m_1+1,m_2+1}(-u-1,-1), \tag{72}$$

$$\Pr\left(E_1 \cap E_2 \cap E_4\right) = \Pr\left(E_2 \cap E_4\right) = \Lambda_{m_1+v,m_2}(1-v,-1), \tag{73}$$

$$\Pr\left(E_1 \cap E_3 \cap E_4\right) = \Pi_{m_1+v,m_2+1}(-v-u,-v), \tag{74}$$

$$\Pr\left(E_1 \cap E_2 \cap E_3 \cap E_4\right) = \Pr\left(E_2 \cap E_3 \cap E_4\right) = \Pi_{m_1+v,m_2+1}(-v-u,-v+1), \tag{75}$$

where Π is defined in (36). Substituting the above expressions in (29) yields (34).

REFERENCES

[1] S. Sruthy and N. B. Mehta, "Power and discrete rate adaptation in wideband NOMA in frequency-selective channels: A systematic approach," in *Proc. ICC*, May 2023, pp. 5396–5401.

[2] Z. Ding, X. Lei, G. K. Karagiannidis, R. Schober, J. Yuan, and V. K. Bhargava, "A survey on non-orthogonal multiple access for 5G networks: Research challenges and future trends," *IEEE J. Sel. Areas Commun.*, vol. 35, no. 10, pp. 2181–2195, Oct. 2017.

[3] S. M. R. Islam, N. Avazov, O. A. Dobre, and K.-s. Kwak, "Power-domain non-orthogonal multiple access (NOMA) in 5G systems: Potentials and challenges," *IEEE Commun. Surveys Tuts.*, vol. 19, no. 2, pp. 721–742, 2nd Qtr. 2017.

[4] D. Tse and P. Viswanath, *Fundamentals of Wireless Communication*. Cambridge Univ. Press, 2005.

[5] "NR and NG-RAN overall description; stage 2 (Release 16)," 3rd Generation Partnership Project (3GPP), TS 38.300 (v16.4.0), Dec. 2021.

[6] 3GPP, "NR; physical layer procedures for data," 3rd Generation Partnership Project (3GPP), TS 38.214 (v15.2.0), Dec. 2018.

[7] Z. Yang, Z. Ding, P. Fan, and N. Al-Dhahir, "A general power allocation scheme to guarantee quality of service in downlink and uplink NOMA systems," *IEEE Trans. Wireless Commun.*, vol. 15, no. 11, pp. 7244–7257, Nov. 2016.

[8] Z. Ding, P. Fan, and H. V. Poor, "Impact of user pairing on 5G nonorthogonal multiple-access downlink transmissions," *IEEE Trans. Veh. Technol.*, vol. 65, no. 8, pp. 6010–6023, Aug. 2016.

[9] Z. Ding, Z. Yang, P. Fan, and H. V. Poor, "On the performance of non-orthogonal multiple access in 5G systems with randomly deployed users," *IEEE Signal Process. Lett.*, vol. 21, no. 12, pp. 1501–1505, Jul. 2014.

[10] P. Xu, Z. Ding, X. Dai, and H. V. Poor, "NOMA: An information theoretic perspective," Available on arXiv:1504.07751 [cs.IT], Apr. 2015.

[11] W. Yu, H. Jia, and L. Musavian, "Joint adaptive M-QAM modulation and power adaptation for a downlink NOMA network," *IEEE Trans. Commun.*, vol. 70, no. 2, pp. 783–796, Feb. 2022.

[12] C. Yuan, X. Tao, W. Ni, N. Li, A. Jamalipour, and R. P. Liu, "Optimal power allocation for superposed secrecy transmission in multicarrier systems," *IEEE Trans. Veh. Technol.*, vol. 70, no. 2, pp. 1332–1346, Feb. 2021.

[13] S. Mcwade, M. F. Flanagan, J. Mao, L. Zhang, and A. Farhang, "Resource allocation for mixed numerology NOMA," *IEEE Wireless Commun. Lett.*, vol. 10, no. 10, pp. 2240–2244, Oct. 2021.

[14] X. Li, C. Li, and Y. Jin, "Dynamic resource allocation for transmit power minimization in OFDM-based NOMA systems," *IEEE Commun. Lett.*, vol. 20, no. 12, pp. 2558–2561, Dec. 2016.

[15] X. Ou, X. Xie, H. Lu, H. Yang, and H. Tang, "Energy-efficient resource allocation for short packet transmission in MISO multicarrier NOMA," *To appear in IEEE Trans. Veh. Technol.*, vol. 71, no. 12, pp. 12 797–12 810, Dec. 2022.

[16] T. Assaf, A. Al-Dweik, M. S. E. Moursi, and H. Zeineldin, "Efficient bit loading algorithm for OFDM-NOMA systems with BER constraints," *IEEE Trans. Veh. Technol.*, vol. 71, no. 1, pp. 423–436, Jan. 2022.

[17] J.-H. Tseng, Y.-F. Chen, and C.-L. Wang, "User selection and resource allocation algorithms for multicarrier NOMA systems on downlink beamforming," *IEEE Access*, vol. 8, pp. 59 211–59 224, Feb. 2020.

[18] L. Lei, D. Yuan, C. K. Ho, and S. Sun, "Power and channel allocation for non-orthogonal multiple access in 5G systems: Tractability and computation," *IEEE Trans. Wireless Commun.*, vol. 15, no. 12, pp. 8580–8594, Dec. 2016.

[19] L. Salaün, M. Coupechoux, and C. S. Chen, "Joint subcarrier and power allocation in NOMA: Optimal and approximate algorithms," *IEEE Trans. Signal Process.*, vol. 68, pp. 2215–2230, Mar. 2020.

[20] Y. Fu, L. Salaün, C. W. Sung, and C. S. Chen, "Subcarrier and power allocation for the downlink of multicarrier NOMA systems," *IEEE Trans. Veh. Technol.*, vol. 67, no. 12, pp. 11 833–11 847, Dec. 2018.

[21] Y. Cheng, K. H. Li, K. C. Teh, S. Luo, and W. Wang, "Two-step user pairing for OFDM-based cooperative NOMA systems," *IEEE Commun. Lett.*, vol. 24, no. 4, pp. 903–906, Apr. 2020.

[22] G. Wang, Y. Shao, L.-K. Chen, and J. Zhao, "Subcarrier and power allocation in OFDM-NOMA VLC systems," *IEEE Photon. Technol. Lett.*, vol. 33, no. 4, pp. 189–192, Feb. 2021.

[23] Y. Fu, Y. Hong, L.-K. Chen, and C. W. Sung, "Enhanced power allocation for sum rate maximization in OFDM-NOMA VLC systems," *IEEE Photon. Technol. Lett.*, vol. 30, no. 13, pp. 1218–1221, Jul. 2018.

[24] S. Feng, T. Bai, and L. Hanzo, "Joint power allocation for the multi-user NOMA-downlink in a power-line-fed VLC network," *IEEE Trans. Veh. Technol.*, vol. 68, no. 5, pp. 5185–5190, May 2019.

[25] Y. Saito, A. Benjebbour, Y. Kishiyama, and T. Nakamura, "System-level performance evaluation of downlink non-orthogonal multiple access (NOMA)," in *Proc. IEEE PIMRC*, Sept. 2013, pp. 611–615.

[26] Q.-T. Thieu, C.-H. Wang, and H.-Y. Hsieh, "A wideband scheduling method for non-orthogonal multiple access in the Vienna LTE-A downlink system-level simulator," in *Proc. IEEE Globecom*, Dec. 2016, pp. 1–6.

[27] F. Liu and M. Petrova, "Dynamic power allocation for downlink multi-carrier NOMA systems," *IEEE Commun. Lett.*, vol. 22, no. 9, pp. 1930–1933, Sept. 2018.

[28] J. Francis and N. B. Mehta, "EESM-based link adaptation in point-to-point and multi-cell OFDM systems: Modeling and analysis," *IEEE Trans. Wireless Commun.*, vol. 13, no. 1, pp. 407–417, Jan. 2014.

[29] Z. Ding, M. Peng, and H. V. Poor, "Cooperative non-orthogonal multiple access in 5G systems," *IEEE Commun. Lett.*, vol. 19, no. 8, pp. 1462–1465, Jun. 2015.

[30] S. N. Donthi and N. B. Mehta, "An accurate model for EESM and its application to analysis of CQI feedback schemes and scheduling in LTE," *IEEE Trans. Wireless Commun.*, vol. 10, no. 10, pp. 3436–3448, Oct. 2011.

[31] S. Lagen, K. Wanuga, H. Elkotby, S. Goyal, N. Patriciello, and L. Giupponi, "New radio physical layer abstraction for system-level simulations of 5G networks," in *Proc. ICC*, Jun. 2020, pp. 1–7.

[32] J. Fan, Q. Yin, G. Y. Li, B. Peng, and X. Zhu, "MCS selection for throughput improvement in downlink LTE systems," in *Proc. ICCCN*, Aug. 2011, pp. 1–5.

[33] S. Boyd and L. Vandenberghe, *Convex Optimization*. Cambridge Univ. Press, 2004.

[34] B. T. Polyak, *Introduction to Optimization*. New York, NY, USA: Optimization Software Inc., 1987.

[35] I. S. Gradshteyn and I. M. Ryzhik, *Table of Integrals, Series and Products*, 4th ed. Academic Press, 1980.

[36] M. Abramowitz and I. A. Stegun, *Handbook of Mathematical Functions with Formulas, Graphs, and Mathematical Tables*. New York, NY, USA: Dover, 1964.